Universidad Zaragoza
1542

Trabajo Fin de Máster

Magnetic measurements of nanometric thin films by means of a new sensor based on diamagnetic levitation

Autor

Mª Rosario Mayoral Blasco

Director

Dr. Javier Sesé Monclús

Facultad de Ciencias

2014

ACKNOWLEDGES

I wish to thanks:

- Dr. Javier Sesé Monclús, my supervisor, for its untiring guidance given to me throughout the research, despite his busy schedule.
- The technicians of the Nanoscience Institute of Aragón (INA), for their permanent scientific and human support

At last but not least, thanks to my lovely parents, Angel and Charo, whom have always been driving force for all my achievements, and to my sisters Susana and María, my brother Javi, my brother-in-law Pablo and my aunt Chari, for their wholehearted support during the time of this research.

INDEX

EXECUTIVE SUMMARY

Within the field pertaining to the measurement of very small quantities of magnetic materials, there are nowadays different devices capable of accurately measuring the weak magnetic fields present in samples under study. Primarily, these devices are based on the technology of SQUID systems (superconducting quantum interference devices) which are able to measure magnetic fields up to 10^{-18} Tesla (T), being the most sensitive magnetometers known till nowadays.

These SQUID devices have a high precision in the measurement of magnetic fields but its use is made in very demanding technical conditions because it needs to incorporate an associated cryogenic cooling system.

Other recent magnetometers, such as SERF based devices (spin-exchange relaxation free devices, based into the exchange of the spin without relaxation) allows also to measure very weak magnetic fields, without resorting to cryogenic conditions, although they can only operate at practically zero fields, being unable to measure higher-intensity fields. Furthermore, their conditions of use are technically demanding, requiring a preheating of an alkali metal vapor and a special medium used to that end associated to the magnetometer.

To avoid the aforementioned inconvenients it is necessary to develop technical alternatives to get accurate measures of weak magnetic fields whose operation requirements don´t need to have technically complex processes prior to the sensing (such as obtaining cryogenic temperatures, vacuum technology or heating sensing atoms), and also involving low manufacturing costs [1].

That is the reason why this master thesis has been developed. On it, the aim is to obtain a high sensitive magnetometer, based on diamagnetic levitation principles, to measure weak magnetic samples. The device comprises a system of two permanent magnets in which one magnet is in a stable equilibrium levitating position by means of the presence of a diamagnetic element being the magnetic study specimen subjected to the action of the magnets of the device. This specimen has been designed and produced by optical lithography in form of microstructures with variable size that will allow to do systematic measurements and to analyze the answer of the sensor. Also, the prototype

has been tested with different measurement strategies and with different geometry as regards to the size of the magnet, magnet-sample distance, and so on. Finally, the measurements done with the prototype have been compared with the one obtained by the high sophisticated technique of the SQUID.

INTRODUCTION

Since the first magnetic needle compass used by the Chinese to improve the accuracy of navigation, many studies have been done to achieve a better knowledge about how the magnetic field acts and to find applications to use it in the real life. Was Hans Christian Oersted, a professor at the University of Copenhagen, who discovered the relationship between electricity and magnetism in 1819. Several other experiments followed. André-Marie Ampère, in 1820, proves that the magnetic field circulating in a closed-path was related to the current flowing through the surface enclosed by the path. In the same year Carl Friedrich Gauss, Jean-Baptiste Biot and Félix Savart, came up with the Biot–Savart law giving an equation for the magnetic field from a current-carrying wire. Later on, in 1831, Michael Faraday found that a time-varying magnetic flux through a loop of wire induced a voltage. James Clerk Maxwell synthesized and expanded these insights into Maxwell's equations, unifying electricity and magnetism into the field of electromagnetism.

Electromagnetism and magnetism knowledge continues to develop, being incorporated into the more fundamental theories of gauge theory, quantum electrodynamics, electroweak theory, and finally the standard model.

As result of all this, the magnetic materials are nowadays divided basically into three types, and gives place to the respective well known magnetic effects: Ferromagnetism, Paramagnetism and Diamagnetism.

1.- Types of magnetic materials

To introduce the different types of magnetism the best way is to describe how materials respond to magnetic fields, having as a basic that the origin of magnetism lies in the orbital and spin motions of electrons and how the electrons interact with one another[2].

- **Ferromagnetic:**

  In these materials the atomic moments exhibit very strong interactions which are produced by electronic exchange forces due to the relative orientation of the spins of two electrons. As a result, the alignment of moments gives place to a large net magnetization even in the absence of a magnetic field (H). This effect is called spontaneous magnetization and is a characteristic of these materials (figure 1a).

  Also, the ferromagnets can retain a memory of an applied field once it is removed. This behavior is called hysteresis and gives place to the well known hysteresis loop, which shows the variation of magnetization (M) with magnetic field as can be seen in figure 1b).

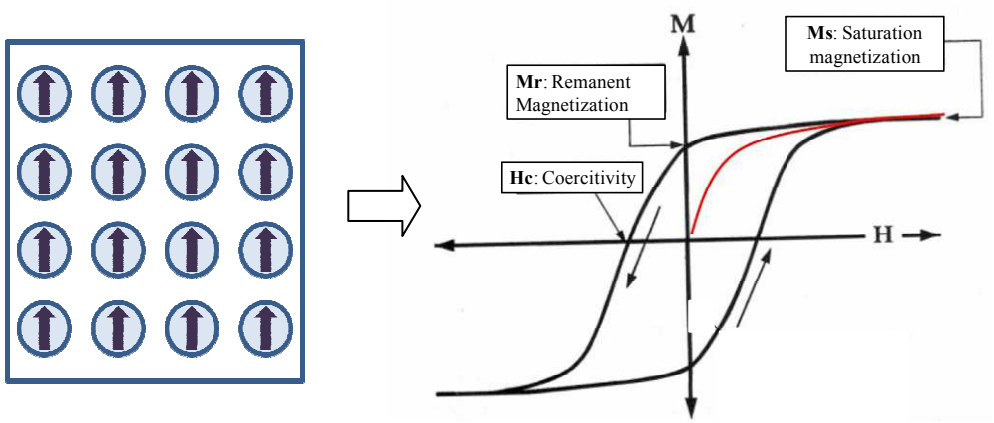

a) Alignment of moments in absence of H.

b) Hysteresis loop.

Figure 1: Ferromagnetic order.

- **Paramagnetic:**

  Paramagnetic materials are composed of atoms or ions that have a net magnetic moment due to unpaired electrons in partially filled orbitals, but they do not interact magnetically having a zero magnetization when there is no field (figure 2a).

  In the presence of a field there is a partial alignment of the atomic magnetic moments appearing a magnetic moment in the direction of the field, resulting in a net positive magnetization and positive susceptibility (χ). This χ is defined as the ratio of M to the field applied: $\chi = M/H$. The efficiency of the field in

aligning the moments is opposed by the randomizing effects of temperature. As a consequence, the susceptibility is temperature dependent. Other characteristic behavior is that when the field is removed the magnetization is immediately lost (figure 2b).

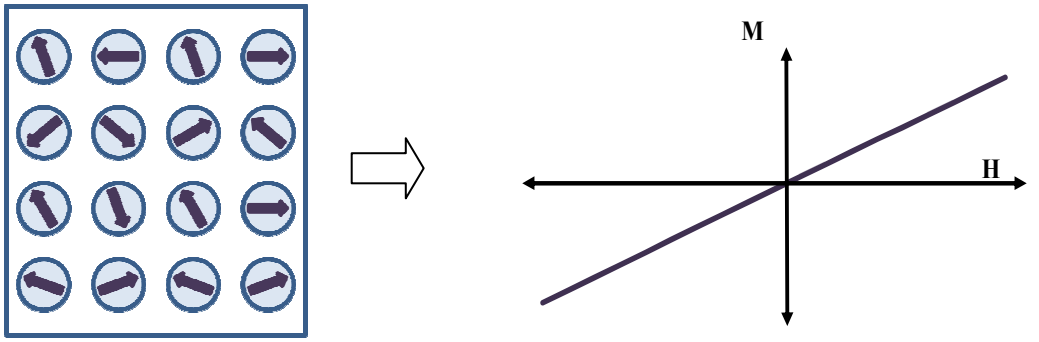

a) Alignment of moments in absence of H.

b) Magnetization (M) curve versus Field (H) applied.

Figure 2: Paramagnetic material.

- **Diamagnetic**

In the diamagnetic substances the atoms have no net magnetic moments because all the orbital shells are filled and there are no unpaired electrons (figure 3a).

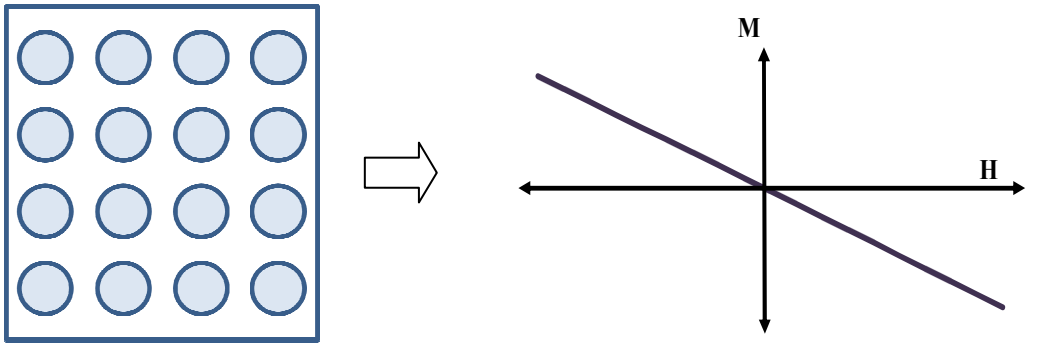

a) Alignment of moments in absence of H.

b) Magnetization (M) curve versus Field (H) applied.

Figure 3: Diamagnetic material.

Diamagnetism is a fundamental property of all matter and is due to the non-cooperative behavior of orbiting electrons when exposed to an applied magnetic field. The magnetic moment is opposite to the field applied and thus the susceptibility is negative (figure 3b). As in the paramagnetic materials, when the

field is removed the magnetization is zero, but here the susceptibility is temperature independent.

2.- History of diamagnetic levitation

Nowadays it is possible to easily levitate diamagnetic substances in the powerful field of rare earth magnets. But the way towards this was long.

It was in the last third of the 18th century when the Dutch Anton Brugmans observed for the first time the phenomenon of diamagnetism while he was investigating the action of a permanent magnet on a plurality of substances. As he investigated bismuth he observed that the piece used for it was repelled by both poles of the magnet.

But was in 1845 when the British scientist Michael Faraday, coin the word diamagnetic to distinguish substances that between the poles of a powerful electromagnet were attracted towards the magnet poles, and others which were moved from stronger points of the field to weaker points. The first one he called "magnetic". The second one "diamagnetic" [3].

Two years later the studies made by William Thomson give place to a doubt about the feasibility of the diamagnetic levitation due to the difficulty of getting a magnet strong enough, and a diamagnetic substance sufficiently light.

It was needed near a century to achieve the technology developed enough to have finally the first demonstration of diamagnetic levitation, which comes in 1939 by the hand of the German physicist Werner Braunbek. He used a strong inhomogeneous magnetic field of an electromagnet to levitate tiny pieces of graphite and bismuth, showing that the Earshaw´s theorem (… *a magnetic body floating in a static magnetic field cannot be in a state of stable equilibrium…)* is invalid for substances with a relative magnetic permeability smaller than unity [4].

After this the dutch Boerdijk repeated Braunbek´s experiment but with a permanent magnet instead of an electromagnet. In this way, he was the first one to demonstrate the levitation of a permanent magnet. His experimental setup was smaller but equalled Braunbek's setup.

The next step to improve the diamagnetic levitation possibilities was given by Dr. Erich Steingroever, who was the first to propose the use of anisotropic graphite for diamagnetic levitation to achieve higher load capacities [5]. On two types of graphite, the Ceylon graphite (a natural graphite mono-crystal) and on the pyrolytic graphite (which is synthezised from purified hydrocarbon gases) the susceptibility perpendicular to the graphite crystal layers is much higher than parallel and also higher than in isotropic graphite. Due to the higher susceptibility the load capacity of the levitating diamagnetic object increases.

Finally, the availability of very strong neodymium iron boron (NdFeB) permanent magnets since the 1990's made possible new developments on the field of diamagnetic levitation [3].

Due to all this was possible that the physicist Andrey Geim and his co-authors research attracted the attention of media and broad public when they levitated living creatures like frogs. This was not only by fun. To obtain these results was first necessary that Geim and M.V. Berry examined extensively the equilibrium conditions needed for levitation of diamagnetic objects in the magnetic field of a solenoid. Stable levitation zones were calculated in detail for different solenoid geometries and different values of the magnetic field. Afterwards an experimental validation followed in the magnetic field of a powerful bitter magnet [3].

The applications of the diamagnetic levitation that appears after all these studies have replaced some uses in the traditional measurements of the microsensors [6] and MEMs accelerometers to measure the earthquakes [7], or the one of the tiltmeters [8] and rotators [9]. Also different fields has been explored like to measure the diamagnetic susceptibility[10] or to manipulate femtodroplets [11]. At the same time patents of a wide classes of systems used to do this experiments have been published [12, 13, 14, 15].

Regarding to this master project the diamagnetic levitation phenomenon has been used to characterize ferromagnetic thin films with nanometric thickness. Using the strong diamagnetism of the pyrolytic graphite and the big BH product that the neodymium iron boron based supermagnets show, it is possible to levitate a supermagnet without the necessity of an external source of energy and at room temperature. This effect of levitation must not get mixed up with the superconductive effect. This last only exists if

the magnetic field does not exceed a critical value which is function of the temperature and is necessary to maintain this temperature at sufficient low values [16].

PRESENT MAGNETIC MEASUREMENT TECHNIQUES

The results obtained with the prototype have been compared with the conventional magnetic measurement technique of the SQUID. As nowadays there are different devices capable of accurately measuring weak magnetic fields present in samples under study, some of the most common so as some emergent ones are explained here.

1.- The SQUID (Superconducting Quantum Interference Device)

It is a magnetometer based on superconducting loops containing Josephson junctions (JJ) and is capable to measure fields as low as 5×10^{-18} T under determined conditions. The technology behind a SQUID´s operation was exposed by Brian Josephson in 1962. He discovered that a superconducting (critical) tunneling current flows between two superconductors separated by a thin layer of insulation, in the absence of any applied voltage [17]. The junction of separation is called the Josephson junction and the value of this critical current through the JJ is affected by the presence of a magnetic field. Depending on the number of Josephson junctions there are two main types of SQUIDs: direct current (DC) SQUID composed of two JJ and radio frequency (RF) SQUID composed of a single JJ. As the first one is more sensitive it is the one explained here.

In the figure 4 is illustrated the working principle of a DC SQUID magnetometer.

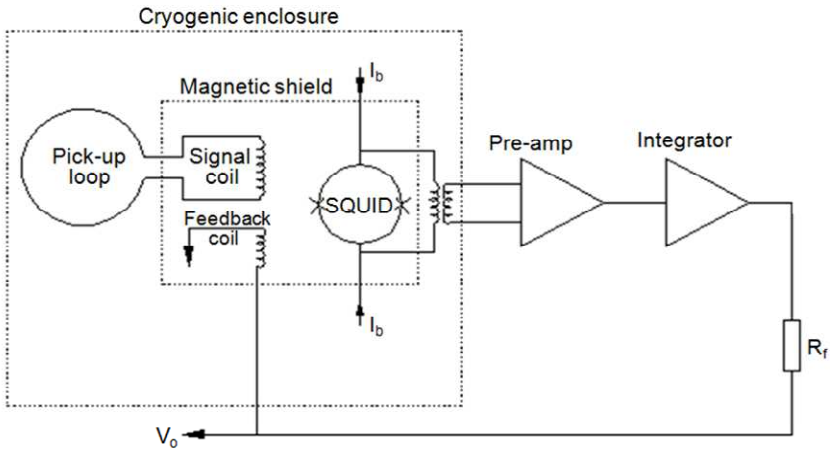

Figure 4: DC SQUID magnetometer operation mode [18].

As can be seen in the figure, the enclosed components in the outer dashed box are kept at a cryogenic temperature (achieved by using a cryogenic cooling system), and are magnetically shielded, except the pickup coil. The rest of the circuitry is left at the ambient temperature.

By applying a DC bias current, Ib to the SQUIDs loop, a voltage is produced across the junctions, which is a periodic function of the sensed magnetic flux through the pick-up loop. Through the feedback coil and a feedback resistor a feedback voltage is produced that helps to maintain a modulated constant flux magnitude within the SQUIDs loop. The output from the integrator presents a linearised response from the SQUID, relative to the sensed flux [18]. By measuring the feedback current it is possible to know the variation in the flux, and therefore the magnetic moment m originating this flux.

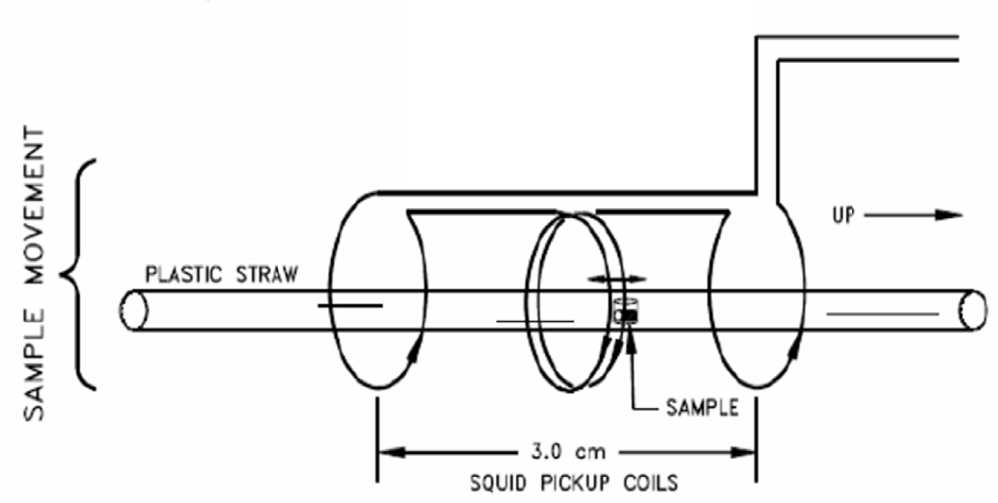

Figure 5: The pickup coils with the sample [19].

To measure the sample, it is placed into the pickup coils inside a plastic straw (see figure 5). The magnetic material influences on the flux of the sensor coil in a proportional quantity to the magnetization of the sample, contributing to the flux or reducing it [19].

The magnetic property measurement system (MPMS) used to obtain the measurements has been the MPMS XL 5T of Quantum Design. The minimum magnetic moment that it is able to detect is of 10^{-10} Am^2 (Amperometer square) whereas the minimum magnetic field is of the order of 10^{-18} T.

2.- The VSM (Vibrating Sample Magnetometer)

The vibrating sample magnetometer measures the magnetization of a small sample of magnetic material placed in an external magnetizing field by converting the dipole field of the sample into an ac electrical signal.

The basic instrument invented by Simon Foner in 1959 is depicted in figure 6. On it, the sample (5) is vibrated perpendicularly to the applied field by the loudspeaker assembly (1), (2), and (4) inducing a voltage in the stationary detection coils (7). This voltage is used to deduce the properties of the sample. A second voltage is induced in a similar stationary set of reference coils (6) by a reference sample (4) which may be a small permanent magnet or an electromagnet. The phase and amplitude of the resulting voltages are directly related because the sample and reference are driven synchronously. Then the magnetic moment of the sample is proportional to the known portion of the voltage from (7), using the voltage from (6) as a reference [20].

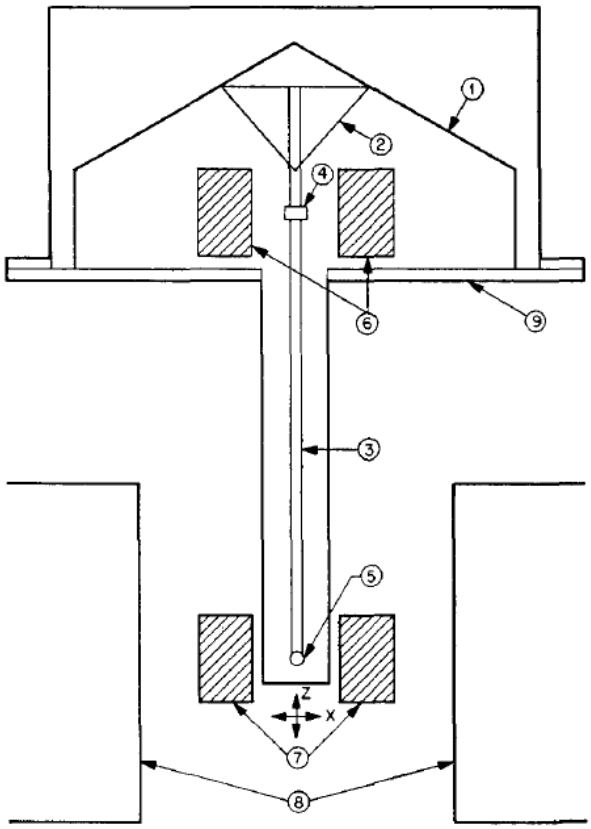

Figure 6: Simplified form of vibrating-sample magnetometer : (1) loudspeaker transducer, (2) conical paper cup support (3), drinking straw (4) reference sample, (5) sample, (6) reference coils, (7) sample coils, (8) magnet poles, (9) metal container [20].

Nowadays the technique has been improved but the basic principle of operation for a vibrating sample magnetometer (a changing magnetic flux will induce a voltage in a pickup coil) remains. Also the basic measurement of the magnetic moment is accomplished by oscillating the sample near a detection (pickup) coil and synchronously detecting the coefficient of the sinusoidal voltage response from the detection coil.

In the VSM systems that are being used today the loudspeaker transducer has been change by a linear motor transport (head) for vibrating the sample. Also the electronics for driving the linear motor transport and detecting the response from the pickup coils has been developed. The rest remains the same [21].

The way of working is as follows: the sample is attached to the end of a sample rod which is driven sinusoidally. The center of oscillation is positioned at the vertical center of a gradiometer pickup coil. By using an optical linear encoder signal readback from the VSM linear motor transport, the precise position and amplitude of oscillation is controlled. Then, the voltage induced in the pickup coil is amplified and lock-in detected in a VSM detection module using the position encoder signal as reference for the synchronous detection. By averaging the in-phase and quadrature-phase signals from the encoder and from the amplified voltage from the pickup coil the final value is obtained.

The system is able to resolve magnetization changes of less than 10^{-9} Am^2 at a data rate of 1 Hz [22].

3.- MFM (Magnetic Force Microscope)

Magnetic force microscopy imaging is a useful technique to locally study the magnetic state of nanostructures. It provides simultaneously information about the topography and the magnetization of the samples.

Usually, their images complete the magnetic characterization performed by standard macroscopic methods such as SQUID or VSM. But other times, it can also be used to give a quantitative value of the magnetization [23, 24] in nanostructures by means of the quantitative MFM imaging analysis as can be seen in the next figure [25].

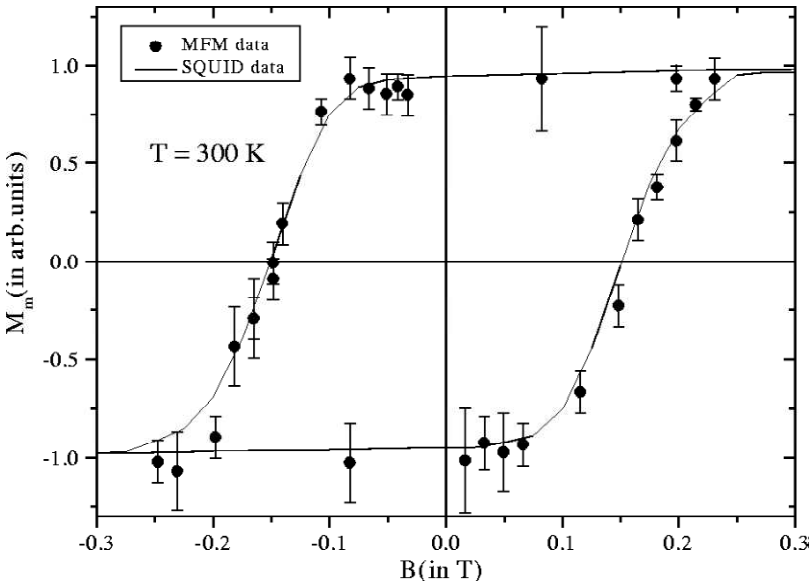

Figure 7: Hysteresis loop of a ferromagnetic sample measured by SQUID magnetometry (solid line). The data points were obtained from the MFM images [23].

For mapping the magnetic forces of the sample the magnetic tip of the MFM interacts with the sample's stray magnetic field. According to Hooke's Law the force (F) detected depends on the spring constant (k) of the cantilever (assuming that the cantilever is oriented parallel to the sample surface) and the variation on the position in the z-axis [26].

$$F = - k\Delta z \qquad (1)$$

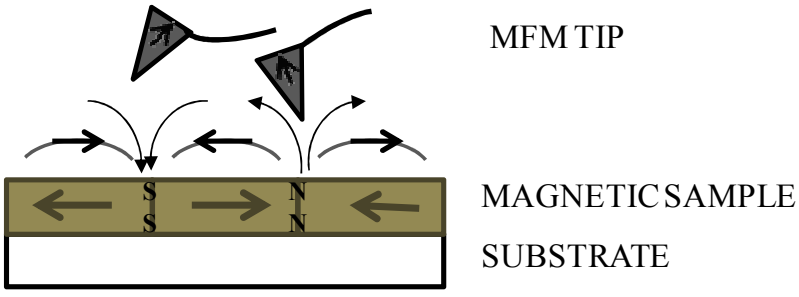

Figure 8: Interaction of the magnetic tip with the sample stray magnetic field.

There are two modes of the tip-sample interaction: static MFM (dc) and dynamic MFM (ac). In the static MFM mode the interaction force is measured through the detection of the cantilever deflection from the equilibrium position, while in the dynamic MFM mode is registered the force gradient, that is to say, the change in resonant properties of

the vibrating system cantilever-sample. The dynamic mode operation is more sensitive to the magnetic field variation than the static one [27].

Since it is based on the force or force derivatives detection, the relation with the energy of tip-sample interaction ($E_{tip\text{-}sample}$) is:

$$\boldsymbol{F} = \nabla \boldsymbol{E}_{tip\ -\ sample} \qquad (2)$$

The $E_{tip\text{-}sample}$ can be expressed in terms of a convolution of the tip stray field H_{tip} and the sample magnetization M_{sample}, where integration is performed over the whole magnetic volume of the sample.

$$\boldsymbol{E}_{\ tip\text{-}sample} \sim \int_{sample} \boldsymbol{M}_{\ sample} \boldsymbol{H}_{\ tip} \qquad (3)$$

Therefore, having measured the forces (or their derivatives) acting between a tip and a sample, it is theoretically possible to restore the magnetisation distribution M_{sample} within an unknown sample upon some model assumptions on distribution of the stray field from MFM tip H_{tip} and having assessed this value numerically[28].

The sensitivity of this measurement technique is found to be in the 10^{-18} Am^2 range under ambient conditions[29]. But it is limited by the tip's magnetic moment and the noise level of the instrument.

4.- SERFs (Spin-exchange relaxation-free) magnetometers

A spin exchange relaxation-free magnetometer is a type of magnetometer developed in the early 2000s. It measures magnetic fields by using lasers to detect the interaction between alkali metal atoms in a vapor and the magnetic field.

The general idea of the method is that light that is near-resonant with an optical transition creates long-lived orientation and/or higher-order moments in the atomic ground state, which subsequently undergo Larmor spin precession in the magnetic field[30]. The modification of the optical absorptive and dispersive properties of the atoms that this precession causes is detected by measuring the light transmitted through the atomic medium.

The resonant medium is usually a vapor of alkali atoms (Rubidium (Rb), Cesium (Cs) or Potassium (K)) contained in a glass bulb. As the depolarization caused by collisions with the cell walls that enclose the atomic vapor limit the spin-relaxation time, cells filled with buffer gas are commonly used. This gas ensures that the atoms optically polarized in the central part of the cell take a long time to diffuse to the walls. The surface relaxation can also be reduced by using a coating on the cell walls that has low adsorption energy for atoms, so they spend less time bound to the surface of the cell. Among such coatings, materials with long chains of hydrocarbons as paraffin work well with alkali metals [31].

Another way to improve the magnetometer sensitivity is to increase the density of alkali-metal atoms. This has been done typically by increasing the temperature of the cell, although alternative approaches using light-induced desorption have been investigated[32].

Regarding to light sources used for atomic magnetometers, originally they were discharge lamps but today the light sources of choice are diode lasers [33].

The atomic magnetometers can be configured so that their output is directly related to the absolute magnitude of the magnetic field through fundamental physical constants. Therefore, no calibration is required.

In the figure 9, a scheme of a general SERF is depicted. As can be seen, the magnetometer consists of a cell containing an alkali vapor and a buffer gas. The alkali vapor is generated by heating a droplet of potassium, rubidium or cesium inside a T-shaped glass cell.

The unpaired electrons on the alkali atoms are spin-polarized by a pump laser (high power diode laser) circularly polarized, pointing the electron spins along the direction of circular polarization. A perpendicular probe laser (single frequency diode laser) detects the orientation of the electron spins as they precess in a magnetic field.

This laser is detuned from the alkali resonance and as it passes through the polarized vapor, the laser polarization angle is rotated due to the circular dichroism of the vapor. The degree of rotation is proportional to the degree to which spins are pointing along the probe beam [34].

To obtain the magnetic field this probe beam is focused onto an array of photodiodes.

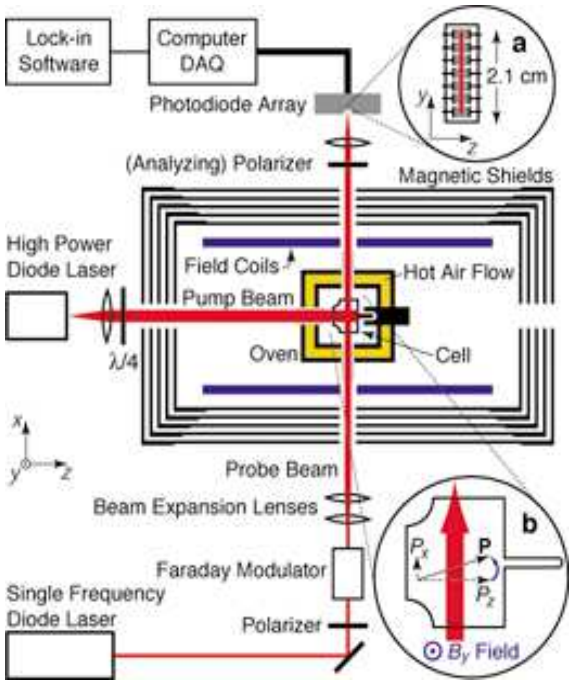

Figure 9: Schematic of a SERF system [34].

As explained before, the SERFs are fundamentally limited by spin-exchange relaxation. Hence, if the spin-exchange collisions happen fast enough and in a sufficiently low magnetic field the spins do not have enough time to precess and decohere between collisions. To achieve these conditions, the oven heats the droplet of alkali in the cell (acquiring the required density), and the shield of the cell from external magnetic fields reduce the precession frequency.

To conclude, the potential capability in sensitivity of this magnetic magnetometer is on the order of 10^{-18} T regarding to the magnetic field.

5.- Nitrogen Vacancy (NV) Magnetometry

The nitrogen-vacancy (NV) color center in diamond has recently emerged as highly versatile optical emitters that exhibit room temperature spin properties. What sets it apart from other color centers is that it is magnetic (i.e., of nonzero spin) and that the luminescence is coupled to the spin state, such that the luminescence intensity can be modulated by magnetic fields [35]. Their remarkable properties include single photon emission, a spin-triplet ground state with long spin coherence time at room temperature, and spin dependent photoluminescence. These properties enable NV centers to locally

detect and measure magnetic fields acting as highly sensitive magnetic field sensors with nanoscale spatial precision [36].

The NV center is formed by removing two adjacent carbon atoms and replacing one of them with a nitrogen atom while leaving the other site vacant. The NV center has been shown to exist in three different electronic forms, the negatively charged NV^-, the neutral NV^0 and the positively charged NV^+. Of them, only the NV^- is magneto-optically active.

The electronic structure of the NV center involves six electrons. Three of them come from the dangling *sp3* bonds of the carbon atoms surrounding the vacancy and other two from the lone pair of electrons located on the nitrogen. The sixth electron is captured from another site in the lattice often coming from other nitrogen impurities, making the overall charge state NV^-.

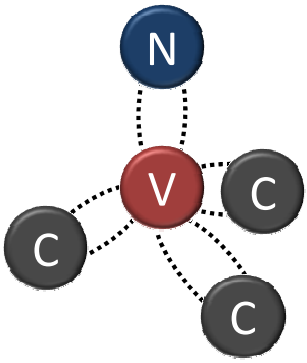

Figure 10: Scheme of a NV center. The dashed lines represent dangling bonds which all overlap in the vacancy. The carbon atoms each contribute one electron , the nitrogen atom contributes two electrons, and one more electron comes from other lattice defects to generate the negatively charged NV center [37].

A simple energy-level diagram of the NV center, is shown in Figure 11. There are various electronic levels in the NV center which includes a ground state |g> of symmetry ^{3}A2, an excited state |e> of symmetry ^{3}E, and a metastable singlet state |s> that involves two levels with symmetries ^{1}A1 and ^{1}E. As two out of six electrons are unpaired, the spin states of ground and first excited states are both triplet states (S=1) and are further split into three spin sublevels.

Because the NV center is not spherically symmetric, the two m_S= ±1 states are degenerate, and the m_S =0 state is energetically lower. The ground state zero-field splitting (ZFS) energy is given by D=2.87 GHz whereas the energy difference between

spin sublevels is D=1.42 GHz for the excited state. Thus, a transition from ms = 0 to ms= ±1 can be achieved by absorption of microwaves at around 2.87GHz.The spin-lattice relaxation time, $T1$, gives the transition rate between m_S =0 and m_S= ±1 sublevels and is of a few milliseconds at room temperature. Finally, by applying magnetic fields the m_S=±1 levels shifts in opposite directions (Figure 11, inset).

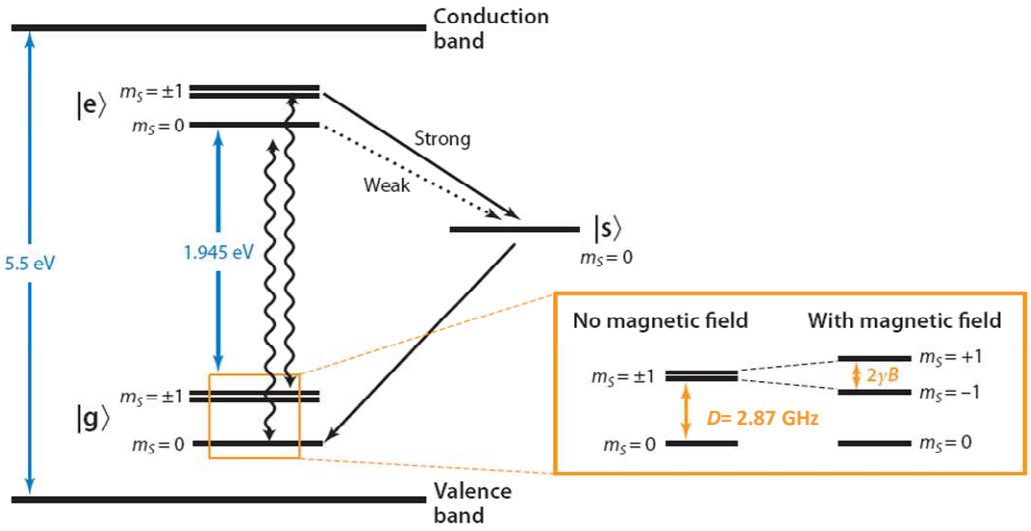

Figure 11: Energy-level diagram of the NV^-. |g>, |e>, and |s> denotes the electronic ground state, the electronic excited state, and the metastable singlet state respectively. Wiggly arrows indicate the radiative transition, whereas the black arrows indicate strong and weak nonradiative decay via the singlet state. The inset depict the three spin sublevels with m_S = 0 and m_S = ±1 at zero and nonzero magnetic field B. D is the zero-field splitting and 2γ B is the Zeeman splitting, where γ is the electron gyromagnetic ratio. By convention, the lower energy transition is associated with ms = −1 [35].

The metastable singlet state |s> is mainly populated from |e, m_S= ±1> owing to differing crossover rates (Figure 11), what implies a pivotal role in the magneto-optic behavior of the NV center. An electron in the |e, m_S= ±1> state decay via the long-lived singlet state, whereas an electron in |e, m_S =0> mostly decays via the fast radiative transition leading to an optical contrast between the m_S =0 and m_S= ±1 states of approximately 30%. Then, the optical emission is seen as fluorescence from the NV center, and a change in fluorescence gives information about the spin state. The promotion to either the ms = +1 or ms = -1 states can be detected by a decrease in fluorescence [38].

To obtain the magnetic field is used the EPR (electron paramagnetic resonance) by

slowly sweeping an auxiliary microwave field. As the microwave frequency is resonant with the EPR transition the fluorescence intensity is reduced due to the excitation from m_S =0 to m_S= ±1. This effect, called optically detected magnetic resonance (ODMR), provides a means to modulate the fluorescence intensity dependent on the magnetic interactions of the single electron spin. There are different mechanism by which the ODMR lines in the NV center can be split: the strain, the Zeeman-effect and the hyperfine coupling. Of them, the Zeeman-effect is used here by coupling a static B-field (nominally aligned along the NV axis) to the NV-dipole moment. As the NV dipole is magnetic it wants to align itself to the applied magnetic field. The three spin states, m_S=+1, 0, -1 correspond to the dipole being oriented directly along, perpendicular to, and directly against, the NV axis. Consequently, the energy of the +1 spin state would increase and that of the -1 state would decrease in energy, while the zero state remains unchanged. This leads to a reduction in the frequency for the m_S=0 → -1 transition and in an increase in the frequency for the m_S=0 → +1 transition [37]. Thus, two resonances appear in the ODMR spectrum as a magnetic field is applied. The absorption at this two resonant microwave frequencies yields information about the degree of Zeeman splitting and hence magnetic field. The separation between this two resonance frequencies is given by $2\gamma Bz$, where $\gamma = 2\pi \times 2.8$ GHz/T is the electron gyromagnetic ratio and Bz is the magnetic field parallel to the NV axis. As a result, measurements of the ODMR frequency immediately yield the absolute value of the magnetic field [35].

One aspect of diamond impurities is that they are highly stable, even if the host crystal is only a few nanometers in size. This small size provides numerous opportunities to employ them as local probes to monitor external perturbations, such as magnetic fields, with high sensitivity and spatial resolution. Then, the basic idea is to embed an NV center at the apex of a very sharp tip (<10-nm tip radius) into a scanning device and to scan this tip over the structure of interest. By mapping the position-dependent Zeeman shift of a single defect center, the magnetic field of a magnetic nanostructure is obtained. This Zeeman shift is typically measured by selectively exciting the transition $|0\rangle \rightarrow |-1\rangle$ of the triplet spin ground state with a microwave pulse and reading out population of the $|0\rangle$ spin state optically [39]. Thus, an optical image of the magnetic field of a magnetic nanostructure is obtained by measuring the NV center fluorescence while scanning the tip over the surface. This technique has shown excellent sensitivity to nanotesla changes in magnetic field as well as nanometer spatial resolution in ambient

conditions and is theoretically expected [38] that with a further develop it should achieved a field resolution of 10^{-18} T.

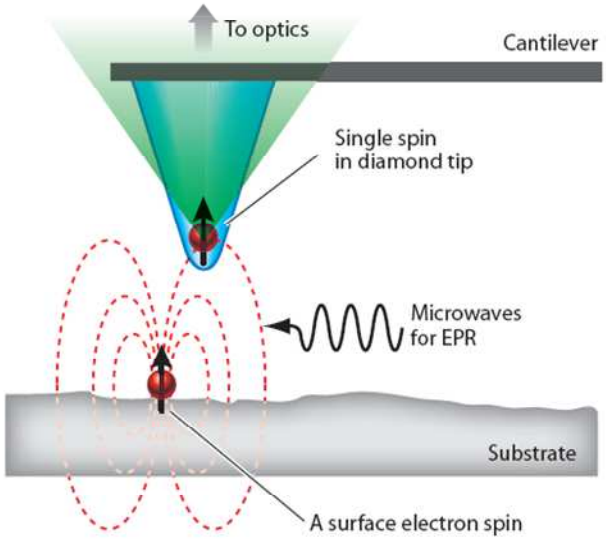

Figure 12: Basic principle of scanning magnetometry. A sharp tip with a NV center at the apex is used to map out the three-dimensional magnetic field vector above a magnetic nanostructure, such as an isolated electronic spin [40].

To sum up this section, the table 1 shows a comparative of the minimum detectable magnetic moment of the MPMS (SQUID system), the VSM and the MFM. As the SERFs and NV magnetometry are recent techniques to measure the magnetic properties, the studies developed till today have been based into the measurement of the magnetic field. This is the reason why their sensitivities are compared here regarding to the magnetic field sensitivity of the MPMS instead of the magnetic moment.

Magnetic measurement technique	Magnetic moment sensitivity (Am^2)	Magnetic field sensitivity (T)
MPMS	1E-10	1E-18
VSM	1E -9	----------
MFM	1E-18	----------
SERF	----------	1E-18
NV magnetometry	----------	1E -9

Table 1: Comparative sensitivities between the different magnetic measurement techniques.

THE TESTED PROTOTYPE

1.- Basics

The main macroscopic behavior of diamagnetic materials is that they are repelled by magnetic fields. This property has been used in this master thesis to obtain a stable and free diamagnetic levitation system, in order to measure ferromagnetic thin films and to characterize its sensibility to nanometric ferromagnetic structures.

To levitate diamagnetic materials the first step is to set up a geometry that can support the object against gravity and at the same time ensure the stability. To achieve it there are two basic approaches: passive or active. The term active is used for systems using a feedback control loop, in opposition to systems levitating passively which do not require any control and do not need any energy. In this project, passive levitation has been chosen due to the simplicity of these systems.

Within the passive levitation there are three basic configurations allowing stable free levitation of permanent magnets [41] as is shown in figure 13.

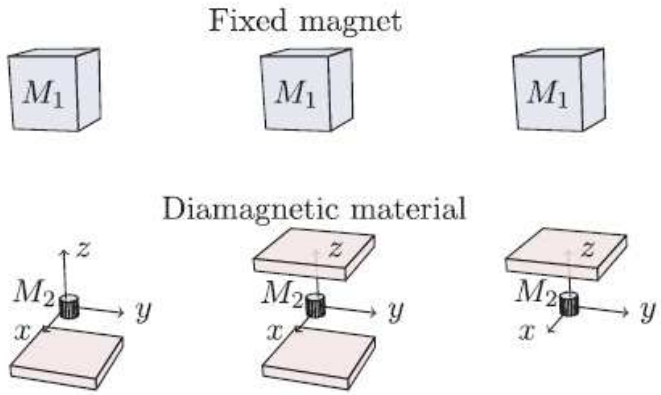

Figure 13: Basic configurations used to achieve passive levitation of a permanent magnet M2 [42].

Looking to the levitation configuration on the left of the figure 13, to stabilize the equilibrium state of the small magnet M2 a diamagnetic material has been placed closely below it. This exercises an upward force of repulsion upon M2 which increases if M2 comes closer to the diamagnetic material. Maintaining M1 and the diamagnetic body without changes on their position, any slighting lowering of M2 from the equilibrium state results in an increase in the repulsion exercised by the diamagnetic body and a decrease of the attraction force between the two magnets M1 and M2. The

sum of both effects is always superior to the weight of M2, making M2 to move up and return to its equilibrium position. In the case that M2 displaces slightly upwards, the magnetic attractive force is more important but the diamagnetic repulsion decreases. The sum of both forces is always lower than the weight of M2 thus M2 moves down. In the two remaining configurations, the diamagnetic levitation works in a similar way [42]. The maximum displacement is typically below one millimeter.

2.- The equipment

As can be seen in figure 14, the equipment comprise of:

1.- The diamagnetic levitation system.

2.- Solenoid.

3.- A magnetic Hall sensor.

4.- The electronic control.

5.- The micrometric gears.

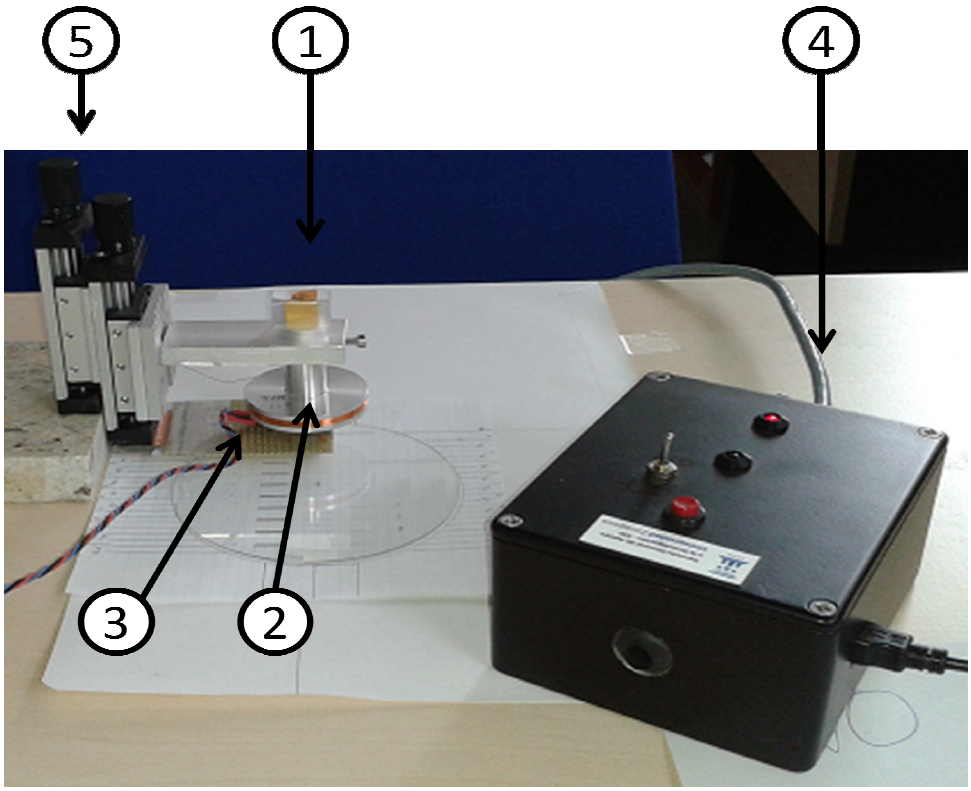

Figure 14: Different parts of the equipment.

2.1.- The diamagnetic levitation system.

The basis of the system is the diamagnetic levitation structure. On it a "magnet 1- diamagnetic substance- magnet 2" configuration has been used (the third structure beginning from the left in the figure 13). The two magnets are NdFeB permanent magnets with a relative size between them enough to obtain their stability under the effect of the diamagnetic material.

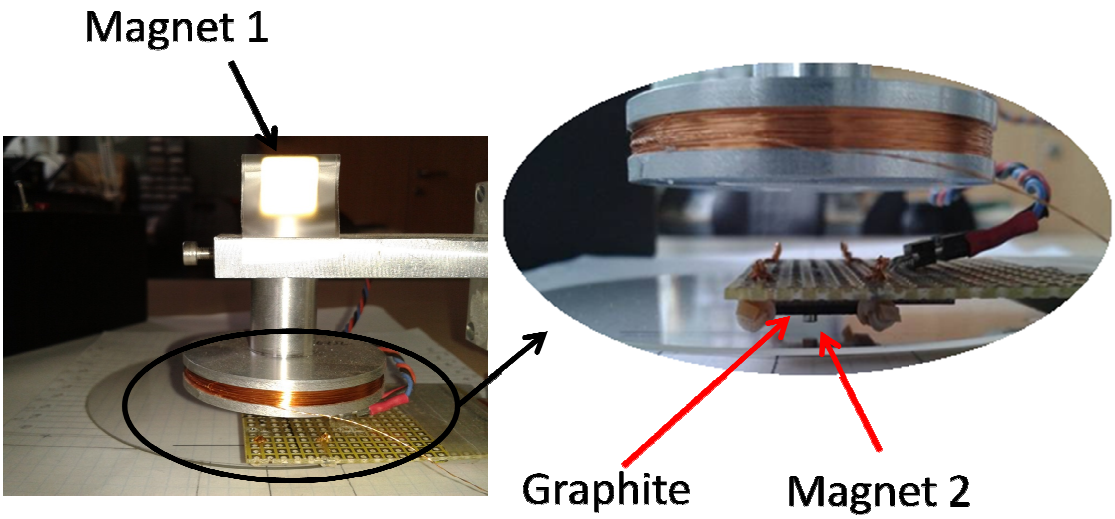

Figure 15: The diamagnetic levitation system.

Magnets

The big magnet 1 (M1) is fixed onto a structure of aluminum (Al) and has a cubic structure of 12 x 12 x 12 mm^3. This is the lifting magnet or, as is often called, the bias magnet. It provides the force necessary to counter gravity.

The second magnet (magnet 2, M2) is the one that levitates and also interacts magnetically with the sample of the magnetic material, object of the measurements. Six magnets with different geometries and sizes have been used in this position. Two of them with a cylindrical shape of 1 mm thickness, being one of them of 1.5 mm diameter and of 1 mm diameter the other. The third has a spherical shape of diameter 3 mm. The last three ones have been cubic magnets with sides 1 mm, 2.5 mm and 3 mm respectively.

Diamagnetic material

As from Earnshaw´s theorem a permanent magnet cannot be levitated by one or more other permanent magnets alone because of instability of the equilibrium position of the magnet, pyrolytic graphite has been used to overcome it. This graphite has the highest diamagnetism of all the diamagnetic materials at room temperature. It has this property because some of its electrons effectively travel in a larger-than-normal orbits.

For a better understanding of this behavior, let´s have a very simple model of the atom to explain it. An electron (as example of all the electrons of the atom) orbiting around the nucleus of an atom of diamagnetic material generates a magnetic field that is just like that of a tiny current-carrying loop of wire. In the natural state this fields are randomly created and they cancel one another doing that the material does not generate a field of its own. But when exposed to an external magnetic field these electrons speed up or slow down so as to oppose the change in the field inside their orbits. The net effect is a repulsive force caused by the induced magnetization that opposes to the applied field [4].

To achieve the great stability in the position of the levitated magnet a horizontal slab of pyrolytic graphite has been chosen because it is strongly repelled by vertical fields but is little affected by in-plane fields.

Hence, the levitation system used works as follows. The permanent magnet M1 attracts the small permanent magnet M2 situated vertically below it. For small horizontal displacements of M2 the equilibrium is stable, whereas for small, vertical displacement is unstable. This lability is overcome by placing directly over M2 a horizontal slab of a diamagnetic body. This latter exercises a downward force of repulsion upon M2 which increases if M2 comes closer to the diamagnetic material or decreases if M2 goes further. As explained before, the sum of forces of the magnet 1 and the pyrolytic graphite balance the displacement of the M2, maintaining the equilibrium. The vertical distance between the magnet M1 and the diamagnetic material can be changed by a micrometric gear, to obtain a stable levitation depending on the magnetization of M1 and M2 and on the susceptibility of the diamagnetic material. This made possible to use different M2 magnets and in this way, to obtain the best response to the sample used.

2.2.- Solenoid

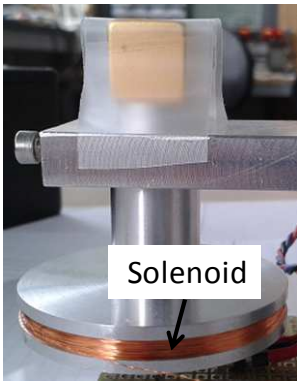

The coil is used to vary the position of the magnet levitated. By its connection to a current generator it creates a field (positive and negative) that interacts with the second magnet in such a way that their stable levitation is overcome, falling down onto the sample to be measured or being restored to the initial equilibrium. By looking at the currents at which these two situations occur is possible to calculate the magnetic moment of the sample.

Figure 16: The coil used to vary the position of the magnet levitated.

2.3.- A magnetic Hall sensor

This sensor is used to measure the displacement of the position of the magnet 2 respect to the equilibrium position. Through this displacement is possible to determine the effect created by the magnetic sample under study. The integrated circuit acts as a transducer, varying its output voltage (the Hall voltage V_H) in a proportional way to the variation of the magnetic field at which are exposed the magnet 1, the magnet 2 the pyrolytic graphite and the magnetic sample.

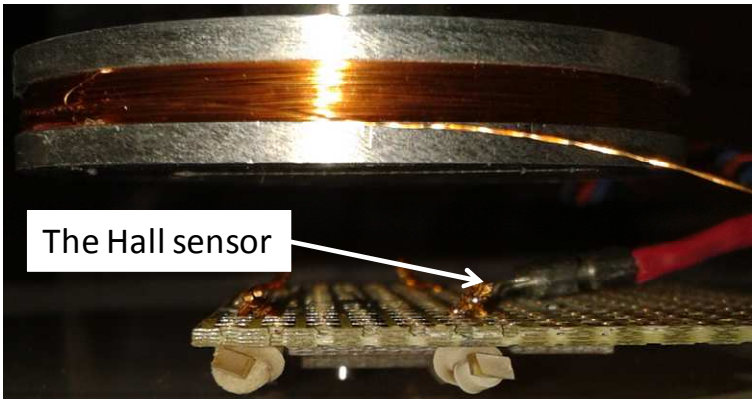

Figure 17: The magnetic Hall sensor

As its name shows it is based on the Hall´s effect. This can be observed when the combination of a magnetic field through a sample and a current along the length of the sample creates an electrical voltage perpendicular to both the magnetic field and the

current. The underlying principle is the Lorentz force, that is, the force on a moving point charge due to electromagnetic fields [43].

The simple theory of the Hall´s effect can be explained as follows. Consider a conducting slab as shown in Figure 18, with length l in the x direction, width w in the y direction and thickness t in the z direction.

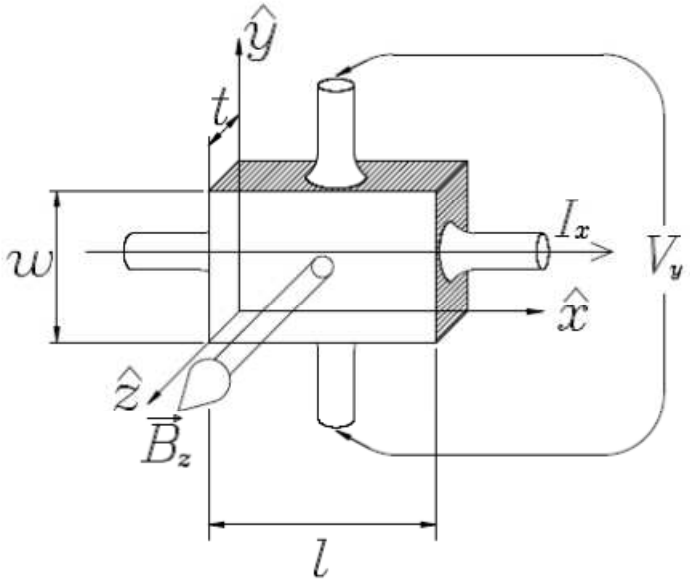

Figure 18: Geometry of fields and sample in Hall´s effect [44].

Assume the conductor to have charge carrier of charge q, number density n and drift velocity v_x (average velocity of the charge carriers over the volume of the conductor) when a current I_x flows in the positive x direction.

Knowing that I_x is equal to the current density J_x multiplied by the cross-sectional area of the conductor wt and as J_x is the charge density nq multiplied by the drift velocity v_x then:

$$I_x = J_x wt = nqv_x wt \qquad (4)$$

Now, assuming that the conductor is placed in a magnetic field perpendicular to the plane of the slab, the charge carriers will experience a Lorentz force q**vxB** that will deflect them toward one side of the slab causing an accumulation of charges along this side which creates a transverse electric field Ey that counteracts the force of the magnetic field.

Since the electrical and magnetic forces on the charge carriers in that direction must be balanced when steady state is reached, there will be no net flow of charge in the **y** direction.

Then:

$$E_y = v_x B_z \tag{5}$$

being E_y the electric field (called the Hall field) in the y direction and B_z the magnetic field in the z direction.

Also, the potential difference across the sample and the Hall voltage V_H is related to the Hall field by

$$V_H = - \int_0^w E_y d_y = - E_y w \tag{6}$$

Thus, from equations (1), (2) and (3) the Hall voltage can be obtained as:

$$V_H = - \left(\frac{1}{nq} \right) \frac{I_x B_z}{t} \tag{7}$$

The term in parenthesis is known as the Hall coefficient (R_H). It is positive if the charge carriers are positive, and negative if the charge carriers are negative [44].

2.4.- The electronic control

The next step to understand the measurements made on this master thesis is to know how works the electronic part involved into the process. It comprises basically a current generator, a Hall sensor control and a microprocessor.

2.4.1.- The current generator

As explained before (section 2.2) this current generator has been used to overcome the stable levitated equilibrium of the second magnet or to restore to it. The schematic of this current generator is shown in figure 19. On it, by means of an instrumentation amplifier (AMP04) a variable voltage VP is obtained whereas the two operational amplifiers of the L272 chip are used to have a fixed reference voltage (VM).

To achieve the desired current a third voltage VO, supplied by a microprocessor, is also involved on the system.

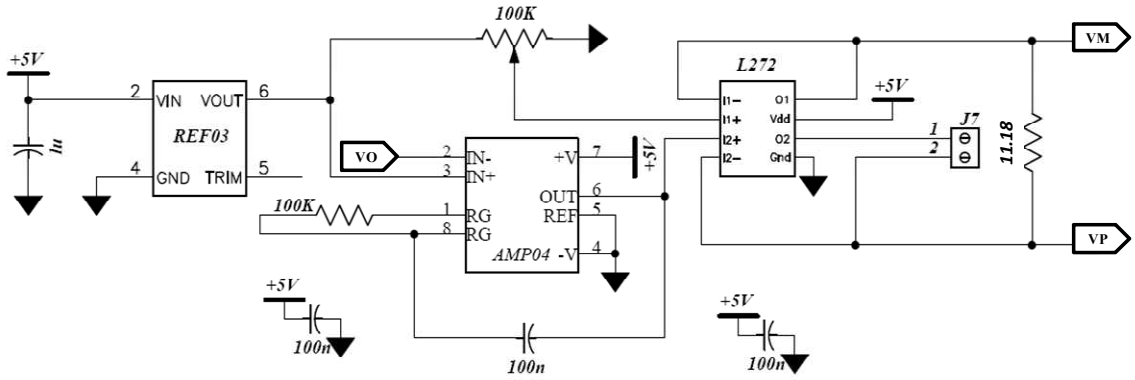

Figure 19: Shematic of the current generator.

Then, to get the variable current the first step is to fix the voltage VM to a value of 1.25V (Volts) by means of the stable reference REF03 and a potentiometer. The second step has been to construct the circuit in such a way that the voltage VP be equal to the difference between the reference voltage 2.5 V given by the REF03 and the voltage VO deal by the microprocessor multiplied by the gain of the instrumentation amplifier. This gain can be calculated by the next formula [45]:

$$\text{Gain} = \frac{100\ \text{K}\Omega}{\text{RG}} \qquad (8)$$

therefore, choosing RG equal to 100 KΩ the gain is 1 and the value of VP follows the equation:

$$\text{VP} = \text{Gain}\ (2.5\ \text{V} - \text{VO}) = (2.5\ \text{V} - \text{VO}) \qquad (9)$$

As the variable voltage VO is given by the microprocessor, the current (i) flowing in the coil is related to the different elements of the circuit by the next equations:

Assuming VO= 0 V:

VM = 1.25 V (fixed)

VP= (2.5 V – VO) = (2.5 V – 0 V) = 2.5 V

By consequence, the maximum current that flows in the coil is defined by:

$$i = \frac{2.5\ V - 1.25\ V}{11.18\ \Omega} = 111\ mA\ (positive\ current) \qquad (10)$$

where the resistor of 11.18 Ω is one chosen as shunt.

Now, assuming VO= 2.5 V:

VM = 1.25 V (fixed)

VP= (2.5 V – VO) = (2.5 V – 2.5 V) = 0 V

Thus, the maximum current able to flow in the coil is:

$$i = \frac{0\ V - 1.25\ V}{11.18\ \Omega} = -111\ mA\ (negative\ current) \qquad (11)$$

Thereby, by the different values of VO inside the range (2.5 V, -2.5 V) given by the microprocessor a variable current in the range (-111 mA, 111mA) will flow in the coil generating the different fields needed.

2.4.2.- The Hall sensor control

The Hall sensor (explained in the section 2.3) detects the variations in field at which are exposed the magnet 1, the magnet 2, the pyrolytic graphite and the magnetic sample. It transforms these measurements into a voltage (the Hall voltage VH) that is correspondent to the different positions of the second levitated magnet respect to its equilibrium. Basically, when there is the maximum of field it gives the maximum voltage whereas at the minimum field is on the contrary.

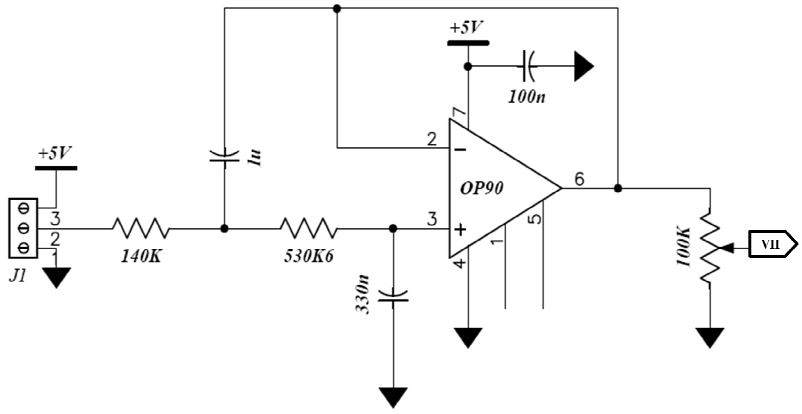

Figure 20: Schematic of the Hall sensor control.

As can be seen in the figure 20, the Hall sensor control adapts these variations to a proportional voltage that is inside the range of voltages that the microprocessor can register. Then, the microprocessor analyze them and gives the correspondent value to the Y axis that will be shown on the screen of a computer by means of the Matlab program chosen as interface. As the operation of the system has been chosen as to have a zero value at the minimum and the maximum voltage at the maximum the middle point is achieved dividing these two values between two. This will help to estimate the magnetic properties of the sample by looking at the variation measurements of the sensor.

2.4.3.- The microprocessor

It is well known that the microprocessor is the chip that controls all the traffic of whatever electronic application, being the nucleus of every complex circuit.

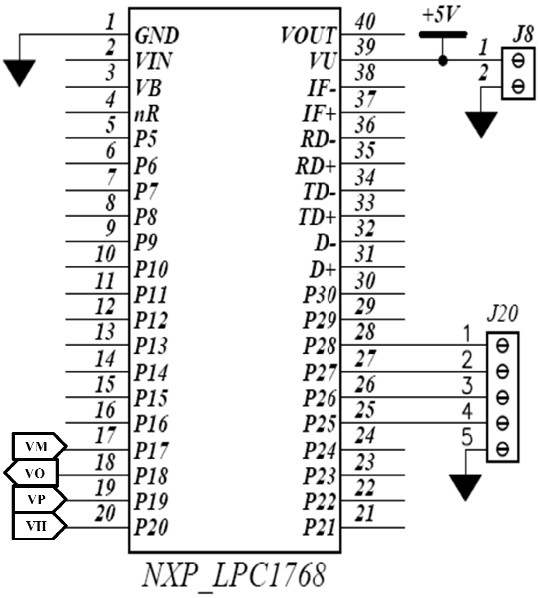

It has been used here to give the variable VO needed to obtain the desirable current flowing through the coil. Furthermore, it reads also the voltages VM, VP and VH making the correspondent logic operations so as to obtain the values of the current flowing in the coil in order to show them into the X axis of the screen of the Matlab program.

Figure 21: The microprocessor.

2.5.- The micrometric gears

Two micrometric gears have been used. One of them, to change the distance between the M1-pyrolytic graphite- M2; the other, to control the distance among magnet 2 and the wafer.

In the first case the aim is to achieve the best stable diamagnetic levitation. In the second, to do possible that the magnetic fields of the sample and the levitating magnet can interact between themselves.

3.-The program

The program used as interface to analyze the measurements is Matlab.

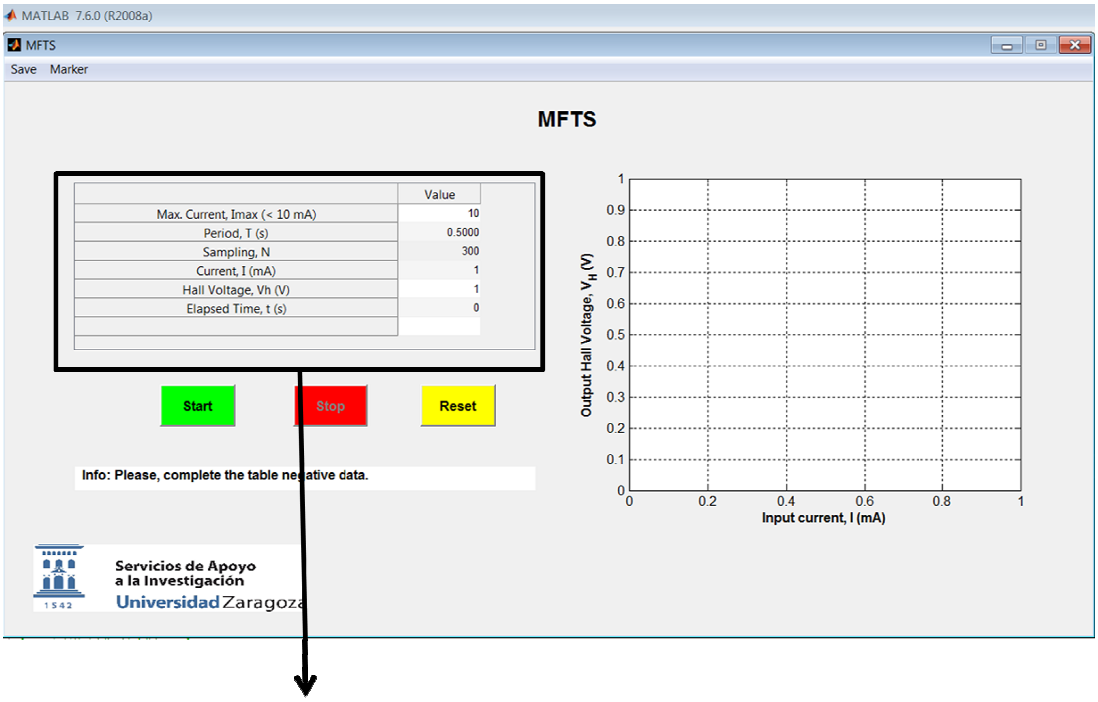

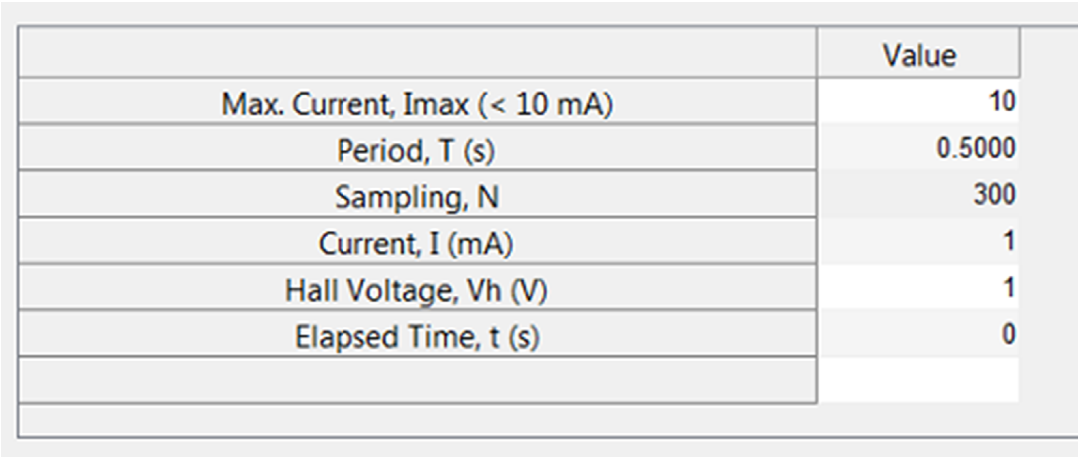

	Value
Max. Current, Imax (< 10 mA)	10
Period, T (s)	0.5000
Sampling, N	300
Current, I (mA)	1
Hall Voltage, Vh (V)	1
Elapsed Time, t (s)	0

Figure 22: Matlab program. Values to choose.

As shows in the figure 22 it is possible to choose the range of current that will flow through the coil by writing it in the value box corresponding to *Max. Current, Imax (<10 mA)*, being 10 milliamp (mA) the maximum in absolute value. The *Period, T (s)* gives the rate in seconds (s) at which the current changes between the maximum and

minimum value during the process and the *Sampling, N* are the number of points (N) displayed into the screen in each complete cycle. The boxes *Current, I (mA), Hall Voltage, Vh (V)* and *Elapsed Time, t (s)* shows respectively during the measurement the values of the current flowing by the coil, the Hall voltage correspondent to these current and the time elapsed from the beginning of the measure.

In the figure 23 is displayed the graph that appears on the screen after the realization of a measurement. On it, the Y axis exhibits the value of the Hall voltage (in Volts) and the X axis the value of the current (in milliamp) flowing in the coil. The system has been connected so that the current at which the levitated magnet falls onto the sample is higher than the current at which the magnet returns to its equilibrium position.

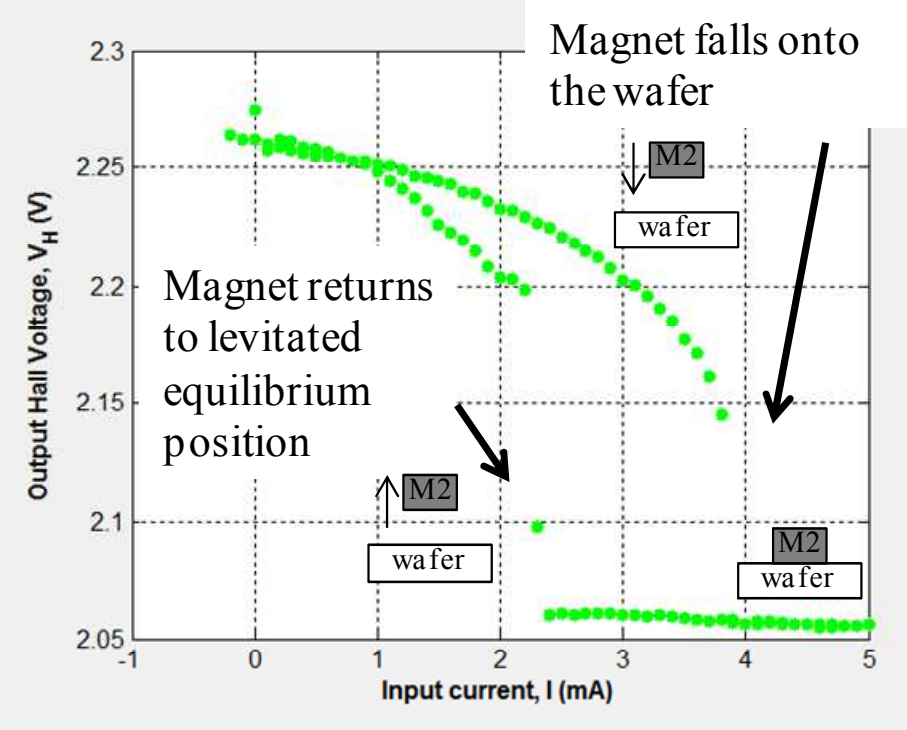

Figure 23: The Matlab program screen shows the fall of the magnet onto the wafer and its recover to equilibrium position.

As the force necessary to recover the equilibrium position of the magnet is higher than the one needed to make it to fall, the current value correspondent to the return to equilibrium position has been chosen to get the final measure. This last is achieved by making the difference between the measure obtained having only the wafer and the one with the sample in order to avoid the magnetic contribution of the substrate.

4.-The wafer (samples)

Finally, to understand the results obtained, is important to know how are the structure used to do the measurements.

In the figure 24 is depicted a picture of the lithography mask used to fabricate the wafer sample.

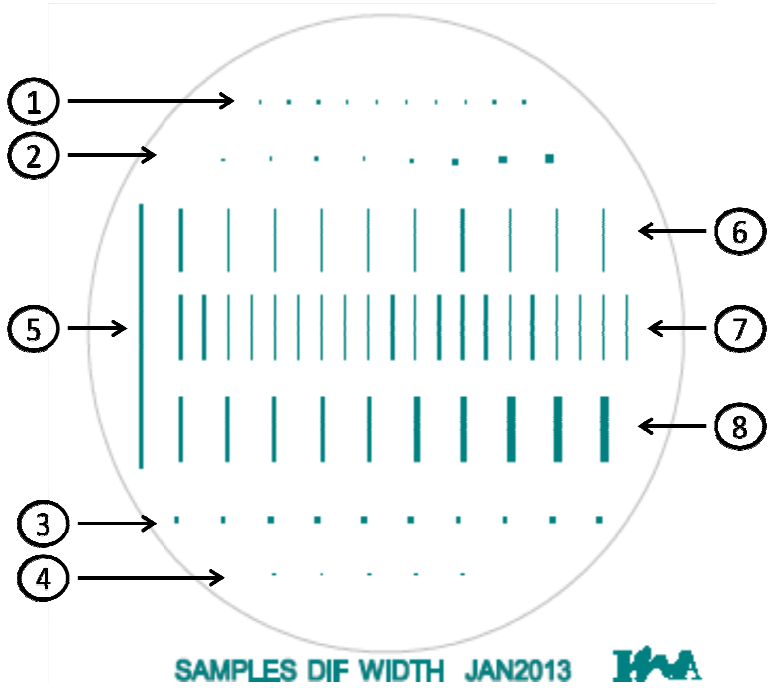

Figure 24: Mask used for the deposition of the magnetic nanometric structures. The circle has a diameter of 100 mm.

As can be seen it comprises a variation of shapes (square and lines) which have also different widths. Their values regarding to width and length in micrometers (μm) goes as follows:

1.- Ten squares of 100 μm x 100 μm.

2.- From left to right, squares of side:

50 μm, 100 μm, 150 μm, 200 μm, 400 μm, 600 μm, 800 μm and 1000 μm.

3.- Ten squares of 500 μm x 500 μm.

4.- Five squares of 200 μm x 200 μm.

5.- A line of 400 µm width x 42000 µm length.

6.- Ten lines of 10000 µm length and a width varying from left to right between 10 µm to 100 µm with an increase of 10 µm each one.

7.- Twenty lines of 10000 µm length and a width varying from left to right between 10 µm to 100 µm with an increase of 10 µm every two. That is to say, they are equal in width every two.

8.- Ten lines of 10000 µm length and a width varying from left to right between 100 µm to 1000 µm with an increase of 100 µm each one.

To achieve the above structures, it has been necessary to use a process of optical lithography known as lift-off because of the nanometric thickness of the samples. The way to obtain them is shown in the next figure.

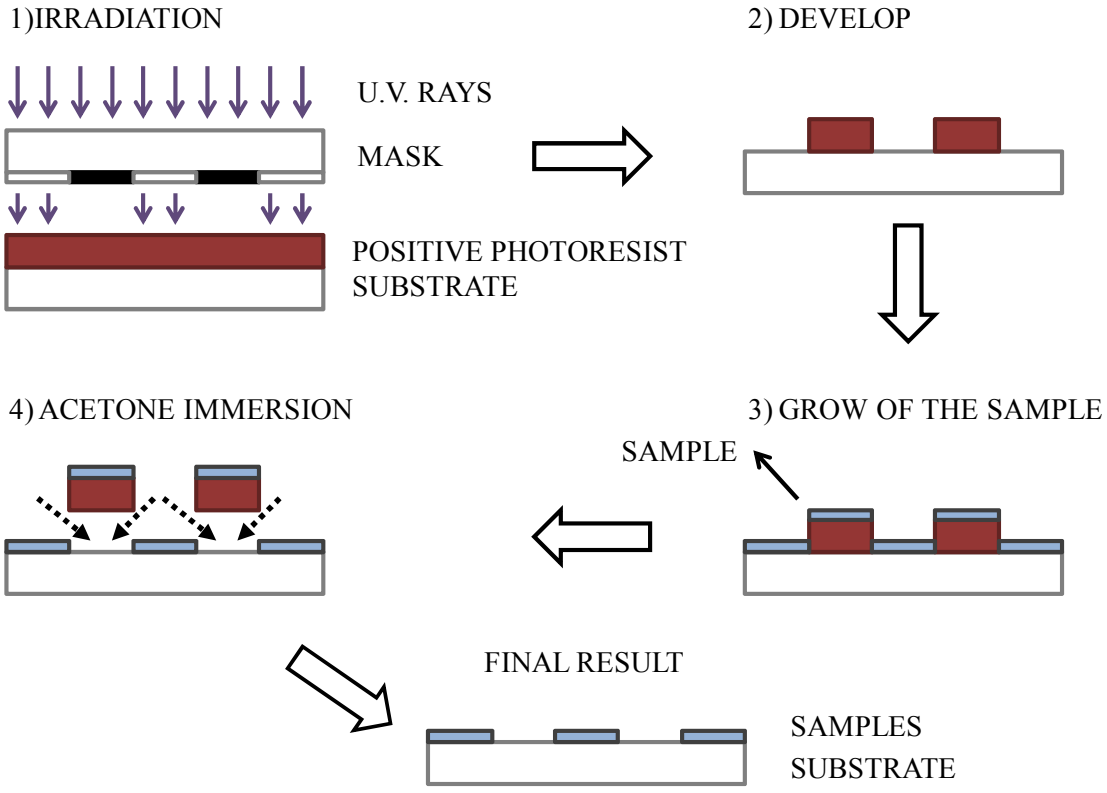

Figure 25: Lift-off process with positive photoresist.

In this lift-off process the first step has been to spin coat the positive photoresist (PR) onto a 4-inch wafer substrate. Next, this PR has been irradiated by U.V. rays through a mask (1) changing the structure of the PR: the bonds between molecules are broken

when exposed, whereas the rest maintained polymerized. By wet chemical develop (2) only the PR in exposed areas is dissolved [46], creating the pattern of the geometry wanted. Then, the ferromagnetic material used for the measurements has been grown onto this pattern (3) by means of an e-beam evaporator. Finally, by immersion of the wafer into acetone (4) the parts with positive PR have been eliminated giving place to the structure of the ferromagnetic nanometric samples desired.

As is well known, the resist used for lift-off processes is usually negative in order to achieve the best profile of the pattern. In the case of the structures that have been produced here, as they have a micrometric size and very small thickness, it is possible to use a positive resist without problem.

To get the results of this master project three different 4-inch wafers have been processed. One of them with a substrate of double side polished silicon (100) and the other two with a substrate of glass. Regarding to the thickness of the nanometric structures, onto the silicon wafer it has been deposited 10 nm (nanometer) of iron (Fe) covered by 10 nm of gold (Au), whereas the two glass wafers have been structured with 20 nm of Fe being covered one of them with 10 nm of Au and the other by 20 nm of Al. This last change of Al instead of Au so as the increase of 10 nm in the quantity of the covering material deposited has been done because of problems of oxidation observed on the first glass wafer.

With regard to the measurements made in this master thesis, by the presence of the magnetic field of the sample in the vecinity of the levitated magnet its position is altered. This convey a correspondent variation on the magnetic field measured by the equipment that gives the possibility to quantify the magnetic properties of the sample by means of a correct calibration of the device.

To conclude, the sensing principle comprises the use of a magnetic material (sample) situated next to the levitated magnet in such a way that the magnetic fields of the sample and the levitated magnet could interact between them. Then, by the comparison between the position of this magnet in absence of sample and in the presence of it, is possible to derivate the magnetic moment of the sample by means of a correct calibration.

MEASUREMENTS

To position the samples under the levitated magnet, five different templates have been made: four of them for the different square samples and the last one for the line samples. This is necessary because the structures are difficult to see by eye.

In all of them, it has been drawn the vertical line correspondent to the location of the line of 400 µm width x 42000 µm length and the horizontal line correspondent to the position of the squares of 500 µm of side.

The next figures show the process to position the sample in the correct location. For example, in the case of the 500 µm side squares:

- The first step is to choose the appropriate template. In this example, the template for the 500 µm side squares.

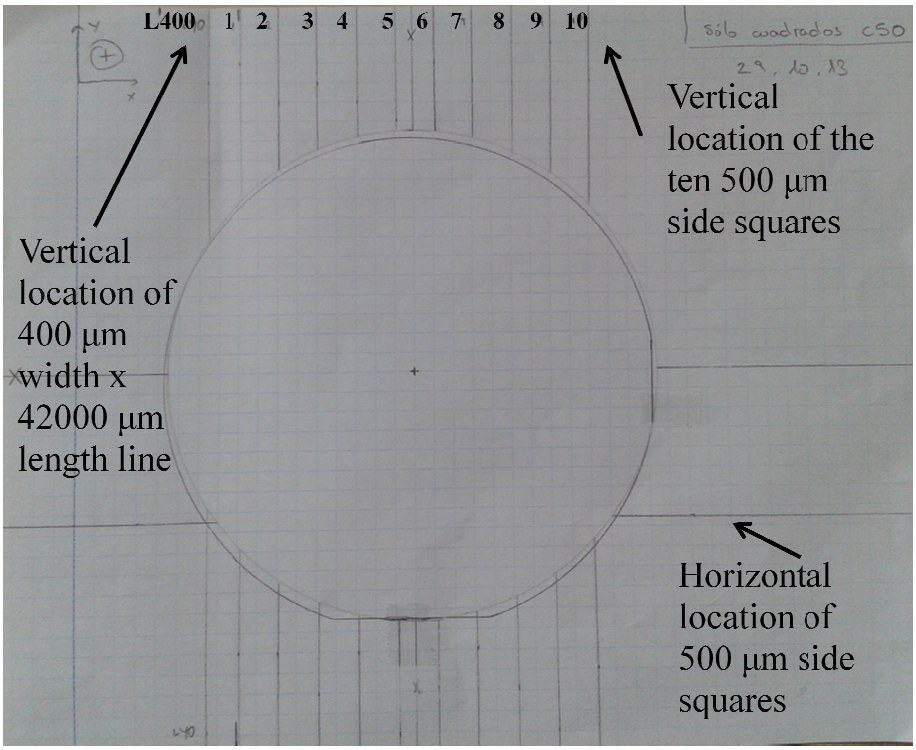

Figure 26: Template for the 500 µm side squares with location lines. The horizontal line in the middle is just to show the center point which has been used to calculate the distance to the location of the 500 µm side squares.

- The second step is to place the wafer in the accurate position by means of the vertical line of of 400 µm width x 42000 µm length and the horizontal line correspondent to the position of the squares of 500 µm of side.

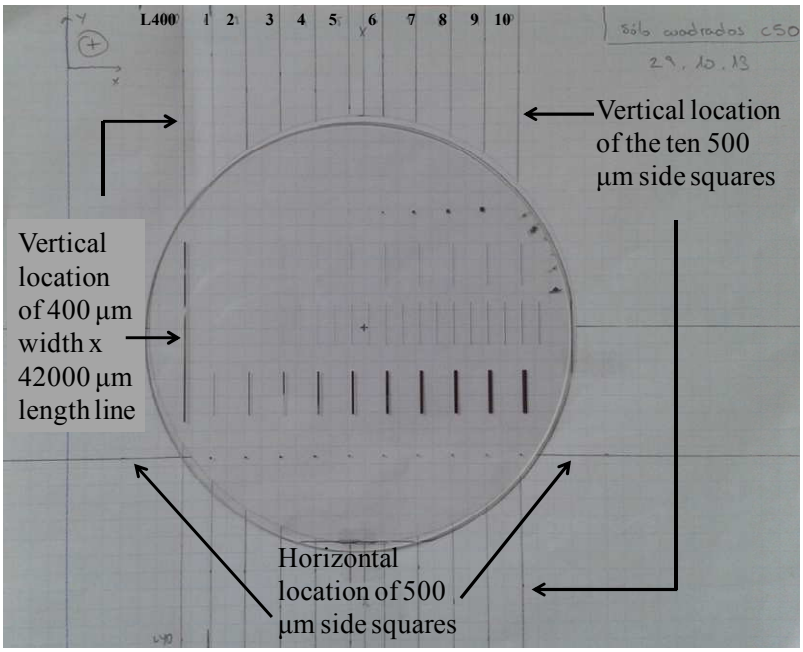

Figure 27: Position of the wafer on the template.

- Finally, the sample is positioned under the magnet by means of the centering lines drawn on the basic template used to locate the magnet M2.

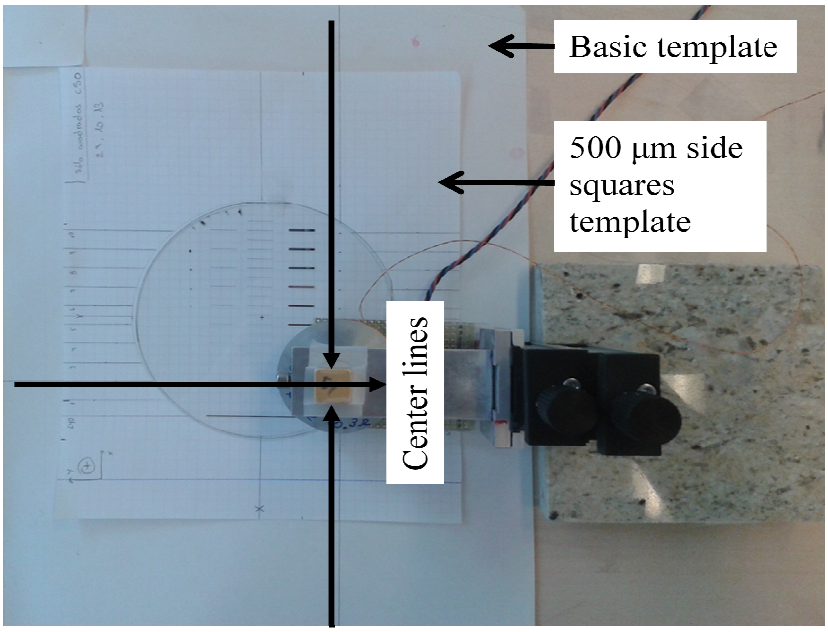

Figure 28: Centering of the template with the wafer regarding to the position of the magnet M2.

Once the samples are positioned under the levitating magnet, the measurement is realized and the data obtained are saved with the Matlab program.

Finally, it is necessary a calibration value to transform the output of the prototype to the magnetic moment due to the magnetic sample. To obtain it, a sample of 49 mm^2 area with a thickness of 20 nm has been measured in a SQUID at 300 K (Kelvin). The sample shows saturation at 1000 Oe (Oersted) and has at this point a value of $1.06x10^{-6}$ Am^2 as can be seen in the figure below.

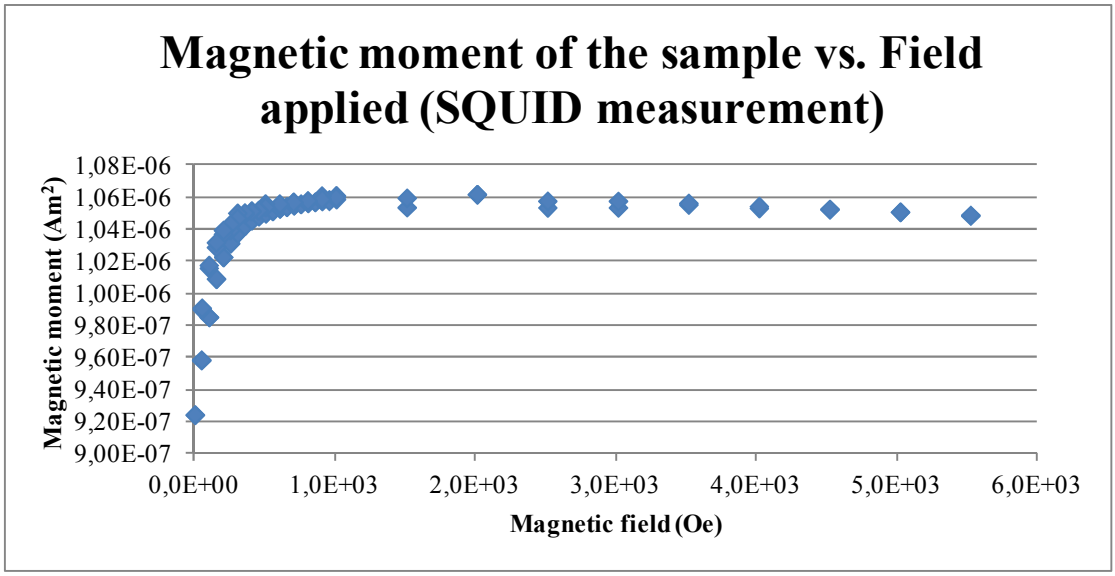

Figure 29: Magnetic moment of a sample of 49 mm^2 area and 20 nm thickness measure with a SQUID at 300 K.

As the magnets of NdFeB used have a magnetic field much larger than 1000 Oe, the magnetization of the samples under its effect is also saturated. Hence, the magnetic moment can be considered as proportional to the area of the sample and thus, the value of the moment regarding to the area of the 400 µm side squares is calculated to be $3.46x10^{-9}$ Am^2.

Then, the calibration value is obtained by dividing this data ($3.46x10^{-9}$ Am^2) by the current obtained for the 400 µm side squares with the cylindrical magnet M2, giving a final data for the calibration of $2.66x10^{-10}$ Am^2 / mA. This calibration depends on the magnet used and the geometry.

The final measurement of the magnetic moment of the structure samples is obtained by multiplying this calibration value by the current measure by the system.

1.- Silicon wafer (100): 10 nm Fe, 10 nm Au.

This wafer has been prepared by depositing 10 nm of Fe covered of 10 nm of Au onto a substrate of silicon (100). The magnet M2 used to obtain the magnetic moment of the structures has been the one with cylindrical shape of diameter 1.5 mm and a thickness of 1 mm.

In the graphic depicted in figure 30 it is shown the value of the current versus the sample width of the lines of 10000 μm length and a width varying from left to right between 10 μm to 100 μm with an increase of 10 μm each one. By looking at these data it is clear that the system has enough resolution to distinguish between the lines, showing also the lineal tendency expected as a function of the width.

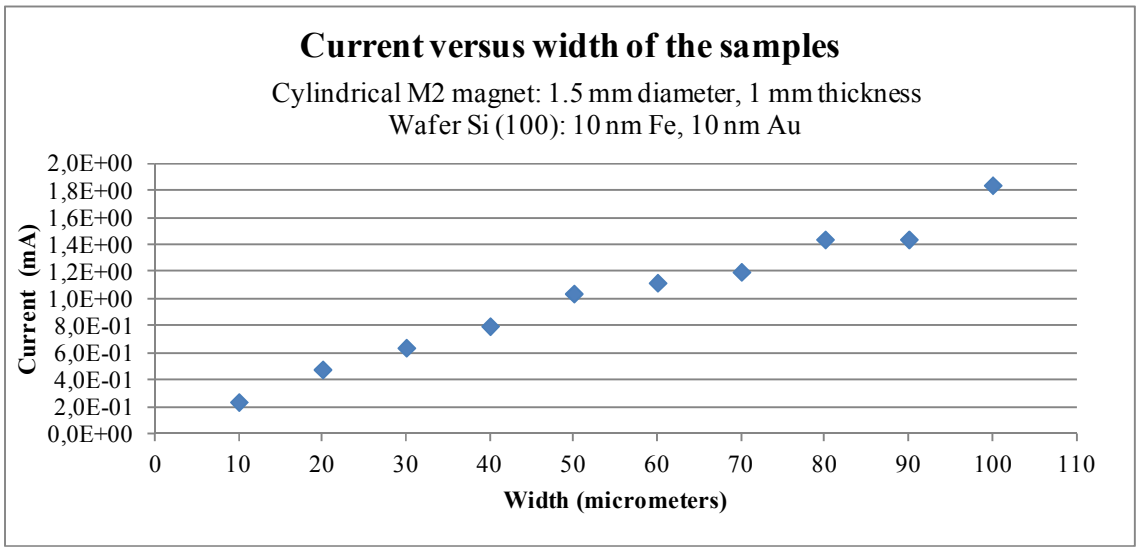

Figure 30: Current versus width of the samples of the silicon wafer (100) using the cylindrical magnet of 1.5 mm of diameter and 1mm of thickness. The width of the lines varies between 10 μm to 100 μm with an increase of 10 μm each one.

To confirm the previous results it has been measured the lines of 10000 μm length and a width varying from left to right between 10 μm to 100 μm with an increase of 10 μm every two (equal in width two at two). The series1 in the graphic of figure 31 shows the values obtained for the lines situated at the left of the twin pair, whereas the series2 are the one situated at the right.

In this case, the linearity is clearly maintained in the lower widths whereas as increasing this width it does not. This effect can be due to the manual positioning of the samples

under the magnet M2 and the small distance between lines what can do that the magnetic moments interfered between lines.

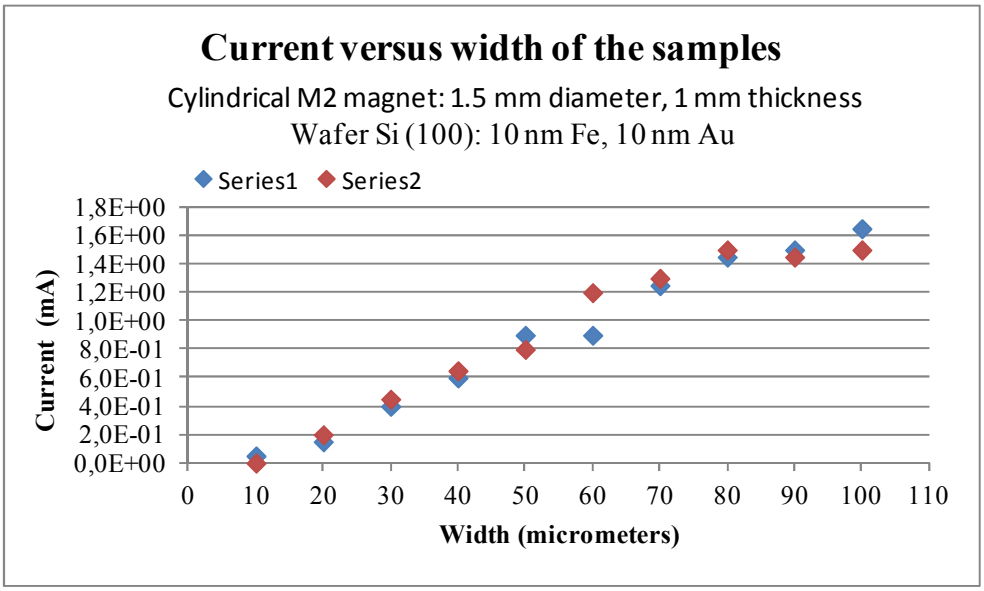

Figure 31: Current versus width of the samples of the silicon wafer (100) using the cylindrical magnet of 1.5 mm of diameter and 1mm of thickness. The width of the lines varied between 10 µm to 100 µm with an increase of 10 µm every two.

The next step continues with the linearity by measuring the lines of 10000 µm length and a width varying from 100 µm to 1000 µm with an increase of 100 µm each one. Figure 32 illustrates the results obtained.

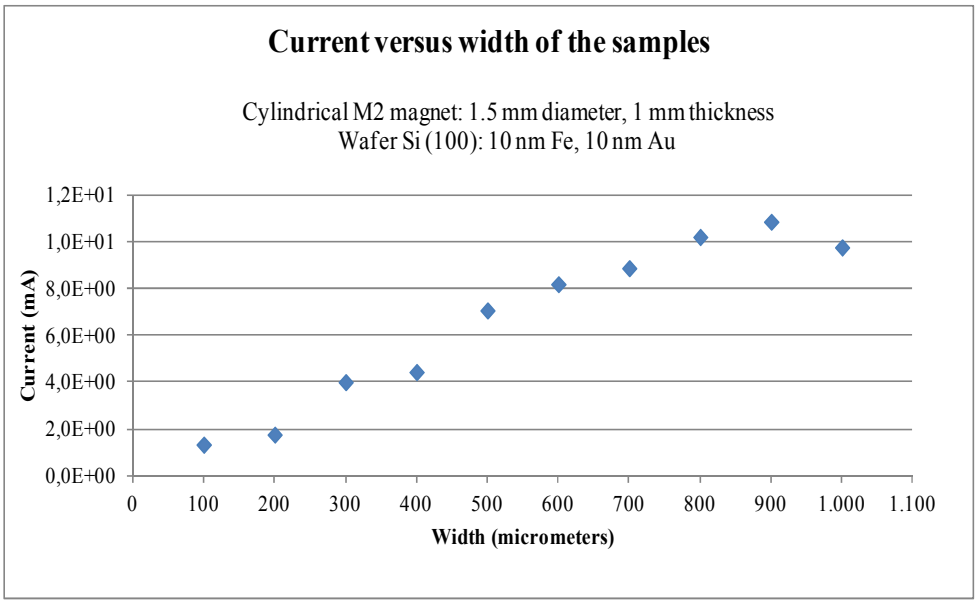

Figure 32: Current versus width of the samples of the silicon wafer (100) using the cylindrical magnet of 1.5 mm of diameter and 1mm of thickness. The width of the lines varied between 100 µm to 1000 µm with an increase of 100 µm each one.

As can be seen, the linearity is conserved except for the line of width 1000 µm that exhibit a decay on the measurement probably due to the interferences with the anterior line because of the proximity between lines.

Furthermore, to test the reproducibility and the resolution of the system the series with squares has been measured. The first were the series with the squares of 500 µm x 500 µm. The next graphic shows that the measurements have a stable behavior varying between them in a maximum of 60 µA. The increase in the numbers of the X axis has been used to distinguish between the equal squares.

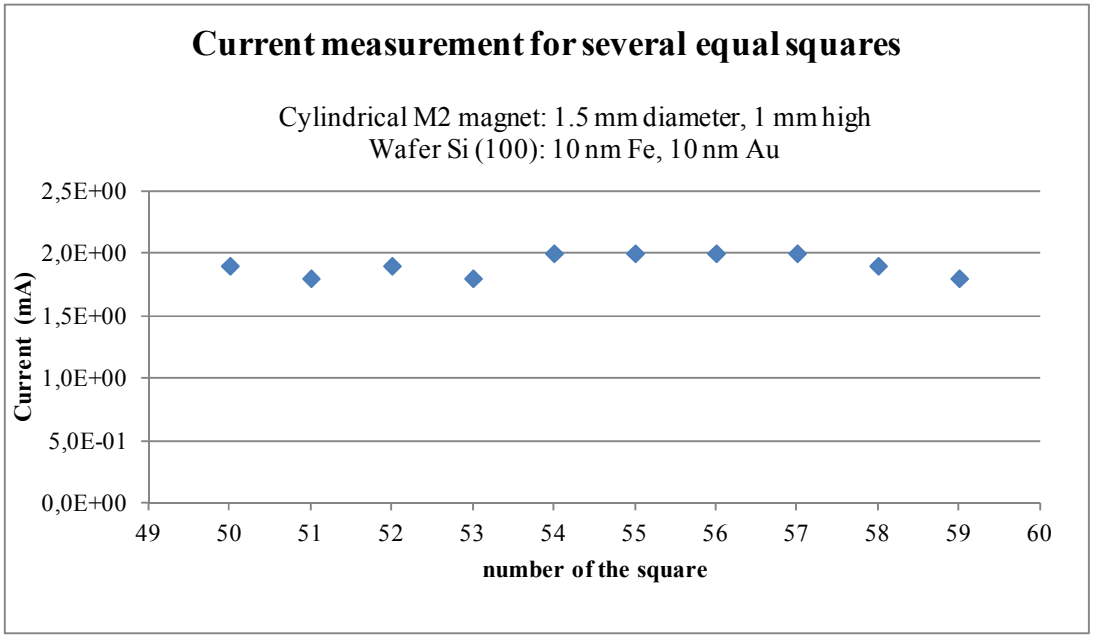

Figure 33: Current versus sample number (all of them are equal fabricated squares) of the silicon (100) wafer using the cylindrical levitating magnet of 1.5 mm of diameter and 1mm of thickness. The samples are squares of 500 µm x 500 µm.

It was not possible to measure neither the squares of 100 µm x 100 µm nor the squares of 200 µm x 200 µm. In consequence, a new wafer has been prepared, changing the silicon substrate by other of glass to improve the visibility of the structures. This has been done in order to achieve better positioning of the samples under the levitating magnet. Also, the thickness has been doubled to look for the sensibility of the system regarding to the material deposited.

2.- Glass wafer: 20 nm Fe, 10 nm Au.

This wafer has been prepared by depositing 20 nm of Fe covered of 10 nm of Au onto a

substrate of glass. The magnet M2 used to obtain the magnetic moment of the structures has been the same of the previous section.

As the linearity of the measurements has been proved before they will not be shown again, centering this section into measurements that displays the doubling of the values because the double deposition of iron and to look if it is possible to see smaller shapes.

The best way to confirm this double correspondence is by comparison of measurements done with the square of 500 µm x 500 µm used in the preceding part.

The comparative graphic depicted below confirms that doubling the quantity of ferromagnetic material deposited the values measured are multiplied by two. As before explained the numbers of the X axis have been chosen to distinguish between the ten different squares.

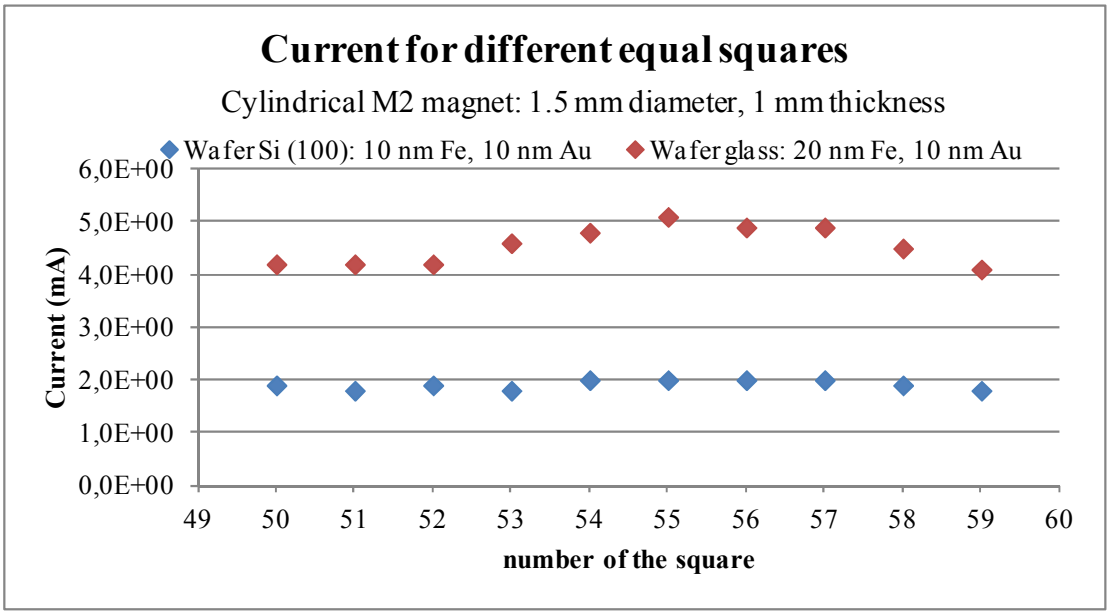

Figure 34: Comparison of magnetic moment versus side of the square samples between the silicon wafer and the glass wafer with the cylindrical levitating magnet of 1.5 mm of diameter and 1mm thickness. The samples are squares of 500 µm side.

There is, however, an increase in the measurement of the squares situated in the middle of the wafer. This is probably due to a higher deposition of material in this zone because of the working way of the evaporator.

Regarding to a possible lower limit compared with the samples of the silicon wafer, it was not possible to determine because of the oxidation of the samples. Hence, a new wafer was prepared.

3.- Glass wafer: 20 nm Fe, 20 nm Al.

This wafer has been prepared by depositing 20 nm of Fe covered of 20 nm of Al. The increase in the quantity of the cover (20 nm instead 10 nm) as the change of material (Al instead Au) has been done to avoid the oxidation of the Fe with the time observed in the previous wafer. As the wetting properties of Al are better than the ones of Au they refill better the possible holes due to evaporation inhomogeneities producing a more compact recover and thus avoiding the possibility of oxygen molecules to react with the Fe.

To continue with the characterization of the prototype, in this section six different magnets with different sizes and shapes has been used to look for the best of them regarding to the sensibility (the one capable to measure the smaller sample). This has been done by measuring the squares with sides 50 µm, 100 µm, 150 µm, 200 µm, 400 µm, 600 µm, 800 µm and 1000 µm and comparing the results obtained with the different magnets.

3.1- M2: cylindrical, diameter 1.5 mm, thickness 1 mm

The first magnet used is the same employed in the previous sections. The results obtained are shown in the next graphic.

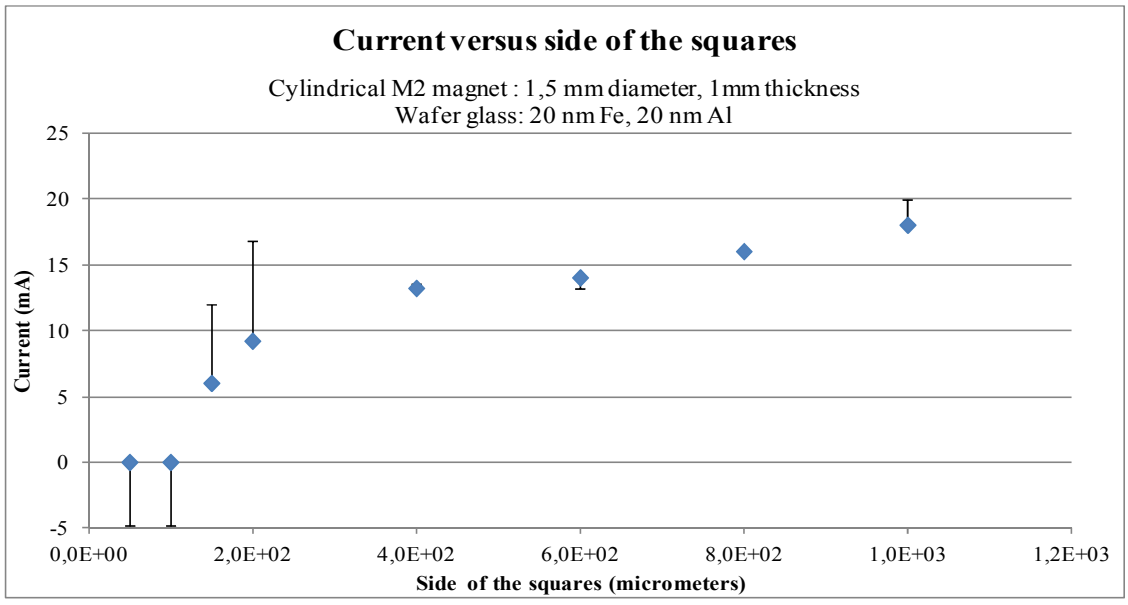

Figure 35: Current versus side of the squares structures with error bars.

The measurements have been made doing two complete cycles to see the reproducibility. As can be seen, the low side squares have a big deviation in the data what means that the system is not able to measure them correctly.

Also the behavior at high sides deviated from the one expected (see figure 36). This shows that from a determined side value of the squares the magnetic moment detected is saturated, giving an upper limit of the size structures capable to be measured depending on the magnet employed.

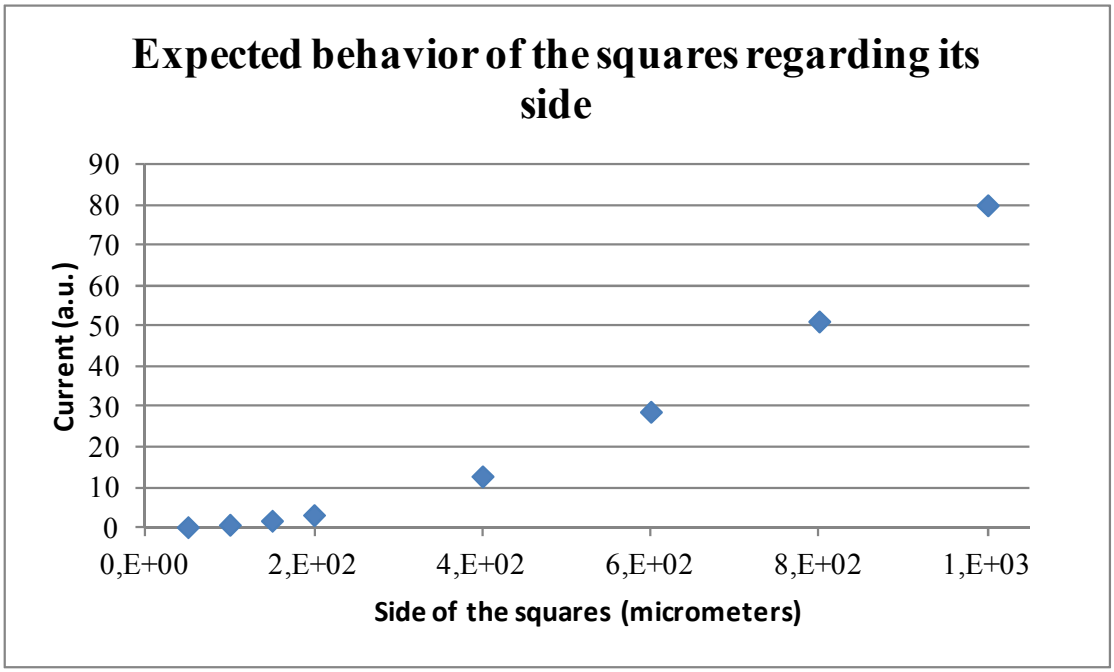

Figure 36: Expected behavior of the squares regarding its side.

Therefore, the measure of the 400 μm can be considered as the lower limit capable to be measured, giving a value of 3.46 x 10^{-9} Am^2 for the magnetic moment.

3.2- M2: spherical, diameter 3 mm

The magnet used here has been a spherical one with a diameter of 3 mm. Due to its spherical shape, it has an effect of rotation when it is over the sample. This rotation affects to the sensor Hall detection doing impossible to obtain any useful data, as can be seen in the next figures that show the behavior under the effect of the substrate without a sample and with the sample of the maximum area (1000x1000 μm^2).

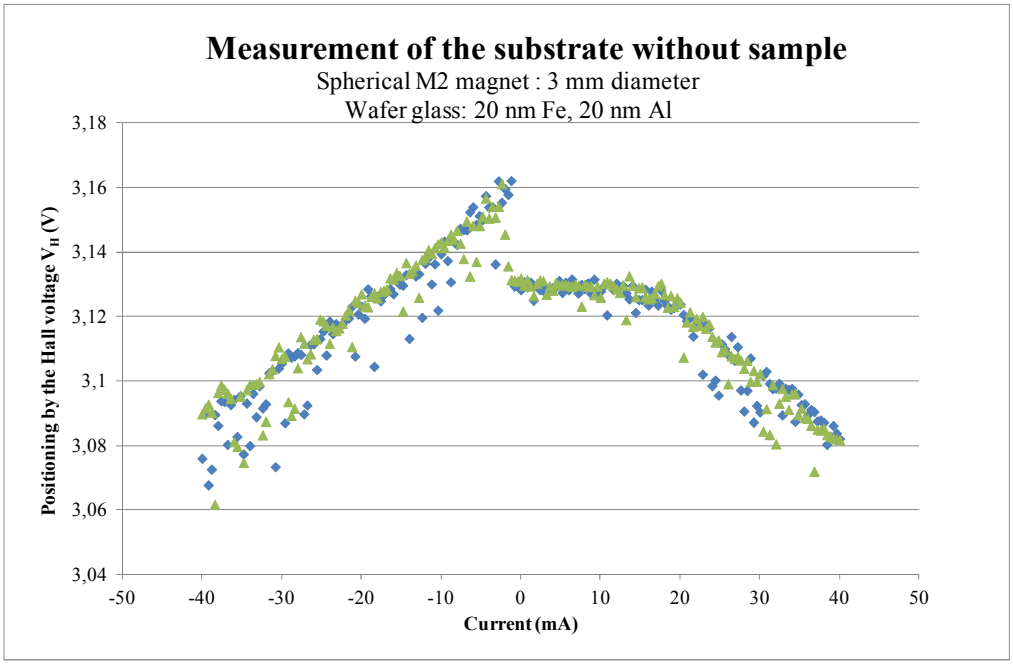

Figure 36: Measurement of the substrate without sample and the spherical magnet of 3 mm diameter.

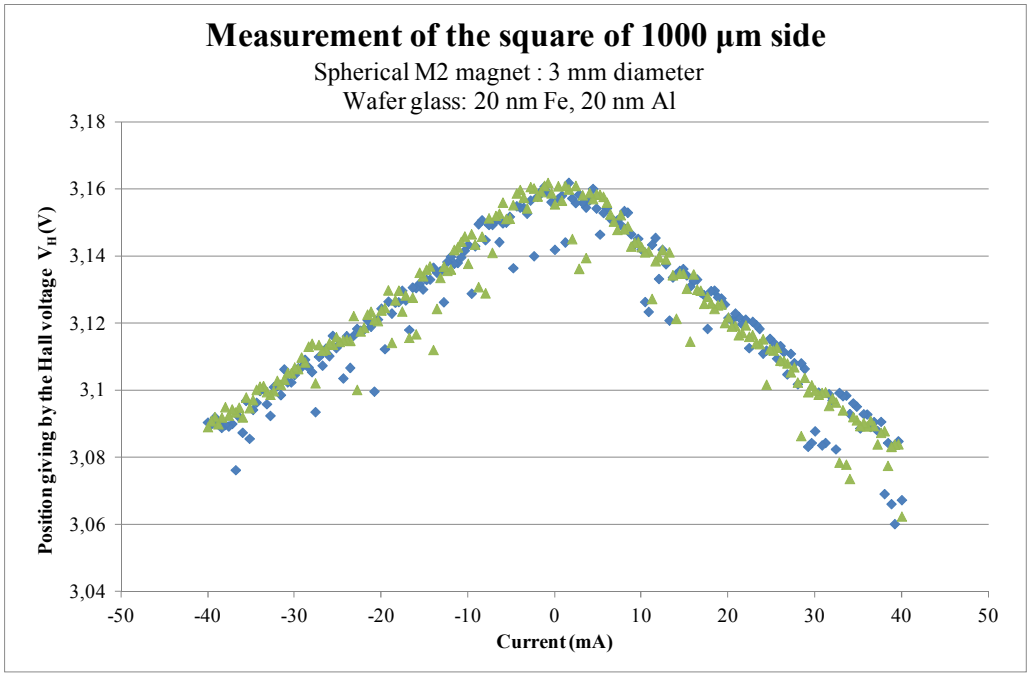

Figure 37: Measurement of the square of 1000 µm side with the spherical magnet of 3 mm diameter.

3.3- M2: cubic, side 1 mm

It has been observed that this magnet rotates during its levitation state doing that sometimes it falls onto the wafer in a non-parallel side position over the square samples.

As a consequence, it can´t interact with all square surface of the bigger samples. However, this is not a problem for the small ones.

Then, to analyze the data in the figure 38 it is necessary to have in mind the position of the magnet over the wafer. On this sense, the square of 1000 µm side has a large error because the magnet recovers its original levitated position the first cycle (where the magnet falls in a non-parallel position) and don´t do the second cycle (the magnet stay over the sample in the correct position). Regarding to the squares of 800, 600 and 400 µm the magnet is over the sample in a perfect parallel location. The samples of 200, 150, 100 and 50 µm are enough small to avoid this problem.

On behalf of the results achieved, the graphic shows that this magnet is able to detect the square of 200 µm side, whereas the negative data of the 50 µm square side is due to the noise of the system.

With all this it is possible to conclude that the lower limit is given by the square of 200 µm side, obtaining a value of the magnetic moment by means of the calibration constant of 8 x 10^{-10} Am^2.

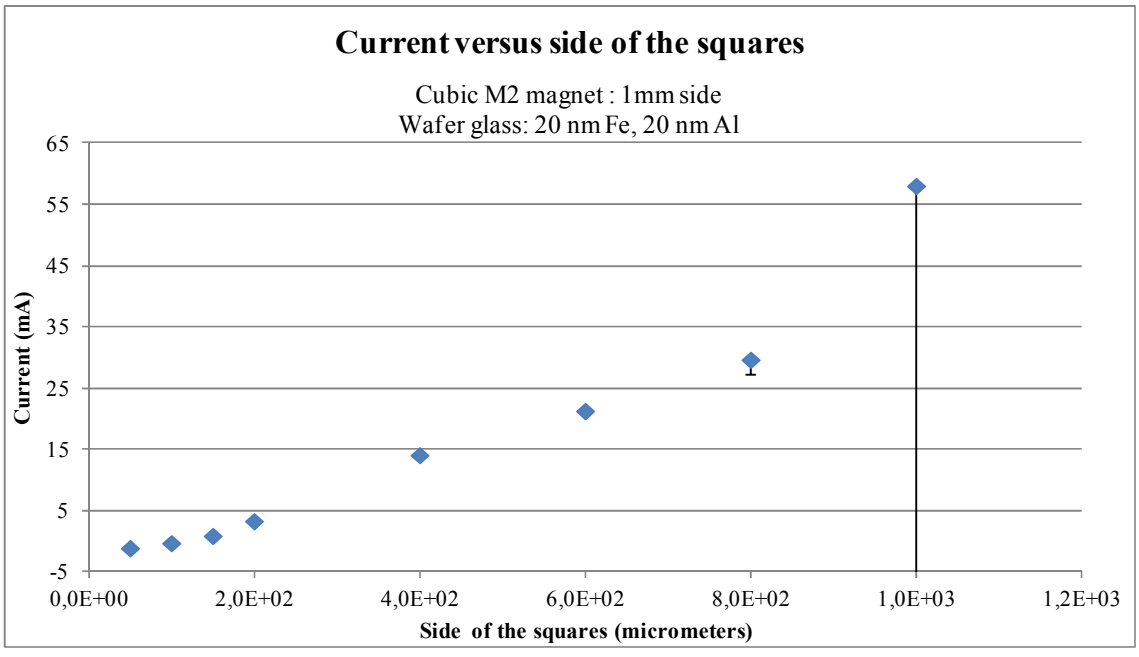

Figure 38: Current versus side of squares with the cubic magnet of 1 mm side.

3.4- M2: cubic, side 2.5 mm

This magnet exhibits a behavior regarding to the data obtained similar to the spherical magnet. Furthermore, it has the rotation effect explained in the section 3.3. The next graphic depict this.

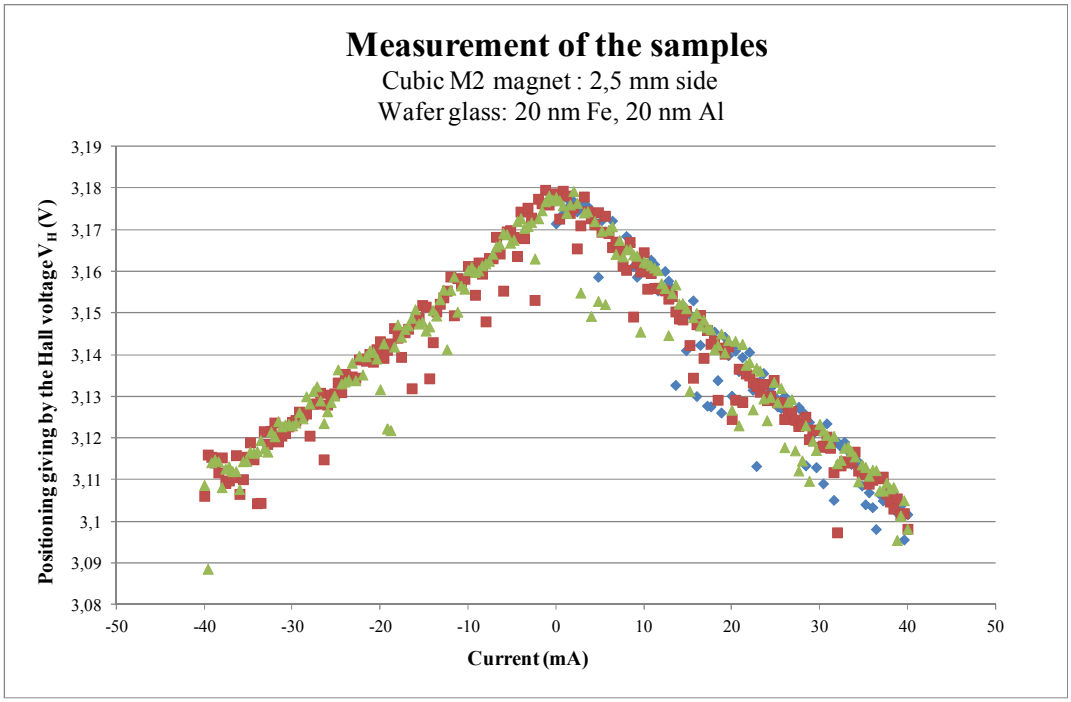

Figure 39: Behavior of the cubic magnet of side 2,5 mm.

3.5- M2: cubic, side 3 mm

As this magnet shows the same characteristics as the one explained before a new magnet has been probed.

3.6- M2: cylindrical, diameter 1 mm, thickness 1 mm

This cylindrical magnet has no problems with the rotation because the axis of rotation is an axis of symmetry of the magnet. Therefore, it has been chosen to compare with the previous results. However, it has been not possible to achieve a position on which the hysteresis loop used to obtain the current at which the system recovers the magnet is null for the non-sample state as displays the figure 40.

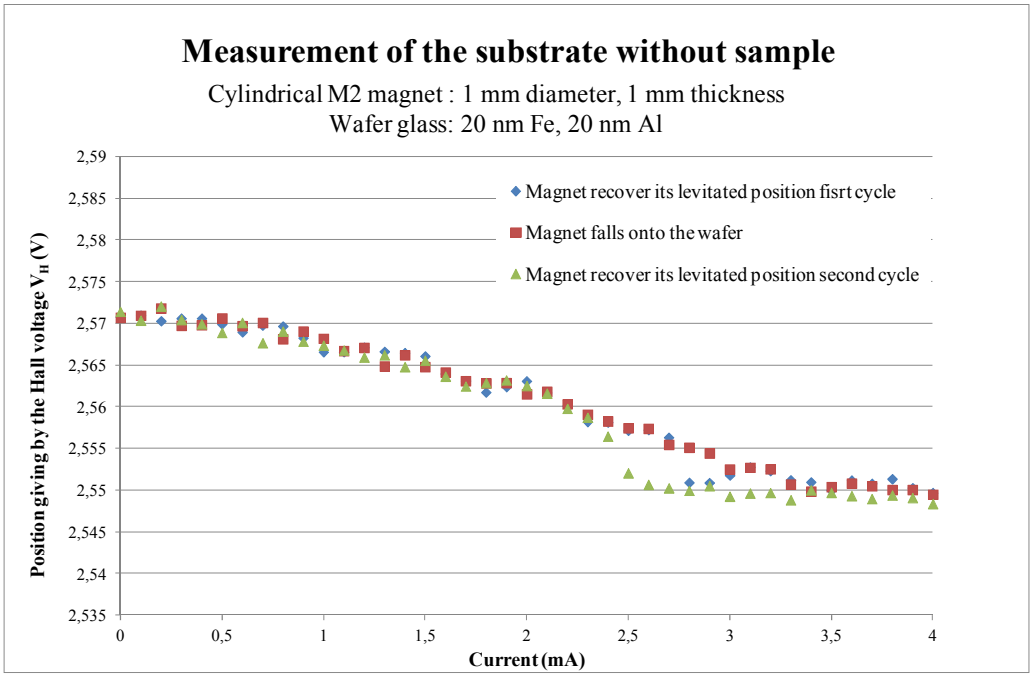

Figure 40: Hysteresis loop of the non-sample state measure by the cylindrical magnet of 1mm diameter, 1mm thickness.

CONCLUSIONS

A new magnetic sensor based on a levitated magnet has been successfully tested. It has been proved to be useful in the characterization of magnetic thin film structures with nanometric thickness.

The measurements done with the cylindrical magnet of 1.5 mm diameter and 1 mm thickness exhibit a good behavior respect to the linearity of the samples as well as a doubling on the values due to the double deposition regarding to the thickness of material.

Respect to the best magnet to be used, is clear that the cubic of 1 mm side gives the best resolution even when its rotation in the levitated state that does it sometimes to fall over the sample in a tilted position makes it unable to be used correctly with samples bigger than 400 μm side.

On behalf of magnets of bigger size, they produce unexpected behavior on the Hall sensor because of its rotation over the sample (as the spherical 3 mm diameter one) or by its rotation in the levitated state (the cubic 2.5 and 3 mm sides ones).

Regarding to this, cylindrical magnets don´t have the effect of perturbation due to the rotation in the levitated state nor the effect of the tilt over the sample. But the relationship between their diameter and thickness need to be controlled in order to achieve a non-hysteresis loop when measuring the non-sample position.

There is also, depending of the size and shape of the magnet used, a moment when a saturation step is reach. This shows an upper limit to have in mind for the structure and quantity of ferromagnetic material of the samples to be measured.

About the prototype itself, it suffers from a problem due to the positioning of the samples under the magnet which now is a manually and delicate operation. It is important to say that smaller the magnet is, bigger the necessity is of an accurate positioning due to the smaller surface covered by it. Then, this is a big handicap to solve to achieve a system easy to be use.

Finally, it has been prove in this master project that the lower limit of detection achieved by the system is of 8×10^{-10} Am^2 at room temperature. This performance is encouraging for a further development to include it in the future into the magnetic moment measurement techniques.

REFERENCES

1. Monclús Sesé, J., Device and method for sensing magnetic materials. **2013,** *Patent WO2013093136 A1*.
2. Moskowitz, B. M., Hitchhiker's Guide to Magnetism. **2002**. http://www.irm.umn.edu/hg2m/hg2m.pdf.
3. Küstler, G., DIAMAGNETIC LEVITATION – HISTORICAL MILESTONES. *Rev. Roum. Sci. Tech.* **2007,** *52*, 265-282.
4. Pelrine, R. E., Diamagnetic levitation. *American Sci.* **2004,** *92*, 428-435.
5. Steingroever, E., Anisotroper diamagnetischer Körper für freie Lagerungen. 1964.
6. Pigot, C.; Chetouani, H.; Poulin, G.; Reyne, G., Diamagnetic Levitation of Solids at Microscale. *Magnetics, IEEE Transactions on* **2008,** *44* (11), 4521-4524.
7. Garmire, D.; Choo, H.; Kant, R.; Govindjee, S.; Sequin, C. H.; Muller, R. S.; Demmel, J. In *Diamagnetically Levitated MEMS Accelerometers*, Solid-State Sensors, Actuators and Microsystems Conference. TRANSDUCERS 2007. International, 10-14 June 2007; 1203-1206.
8. Simon, I.; Emslie, A. G.; Strong, P. F.; McConnell, R. K., Sensitive Tiltmeter Utilizing a Diamagnetic Suspension. *Review of Scientific Instruments* **1968,** *39* (11), 1666-1671.
9. Trénec, G.; Volondant, W.; Cugat, O.; Vigué, J. , Permanent magnets for Faraday rotators inspired by the design of the magic sphere. *Applieds Optics* **2011,** *50*, 4788-4797.
10. Takahashi, K.; Mogi, I.; Awaji, S.; Watanabe, K., Non-contact measurement of diamagnetic susceptibility change by a magnetic levitation technique. *Meas. Sci. Technol.* **2011,** *22*.
11. Lyuksyutov, I. F. Naugle, D.G.; Rathnayaka, K.D.D. , On-chip manipulation of levitated femtodroplets. *Applied Optics* **2011,** *50*, 4788-4797.
12. Heinrich, B., Magnetic Levitation System. **2009,** *Patent US 2009/0160279 A1*.
13. Moser, R.; Sandtner, J.; Barrot, F., Diamagnetic Levitation System. **2006,** *Patent US 2006/0162452 A1*.
14. Hansen, B. N., Method and Apparatus for Magnetic Levitation. **2002,** *Patent US 2002/0124765 A1*.
15. Berstis, V., Pressure Wave Sensor using Levitated Mass. **2004,** *Patent US 2004/0244492 A1*.
16. Boerdijk, A. H., Technical aspects of levitation. *Philips Res. Rep.* **1956,** *11*, 45-56.
17. Daniel, B. Y., Electronic Characteristics of SQUIDs. Unpublished BSc thesis, Massachusetts Institute of Technology. **1998**.
18. Ogunyanda, K., A Superconducting Quantum Interference Device (SQUID) Magnetometer for Nanosatellite Space Weather Missions. Master thesis. Cape Peninsula University of Technology. **2012**.
19. Area de Medidas Físicas- Servicio de Instrumentacion Científica. Universidad de Zaragoza. Curso Técnico Magnetómetros SQUID. **2008**.
20. Foner, S., Versatile and Sensitive Vibrating-Sample Magnetometer. *Rev. Sci. Instr.* **1959,** *30*, 548-557.
21. Vibrating Sample Magnetometer (VSM) Option User's Manual. Quantum Design. . **2011**.
22. EV9 Vibrating Sample Magnetometer data sheet. Microsense. **2010**. *http://www.microsense.net/products-vsm.htm*
23. Sorop, T. G; Untiedt, C.; Luis, F.; Jongh, L.J., Magnetization reversal of individual Fe nanowires in alumites studied by magnetic force microscopy. *J. App. Phys.* **2003,** *67*.
24. Nielsch, K.; Wehrspohn, R.B.; Barthel, J.; Kirschner, J.; Fischer, S.F.; Kronmüller,H.; Schweinböck, T.; Weiss, D.; Gösele, U, High density hexagonal nickel nanowire array. *J. Magn. Magn. Mater.* **2002,** *249*, 234-240.
25. Asenjo, A; Jaafar, M.; Navas, D.; Vázquez, M., Quantitative magnetic force microscopy analysis of the magnetization process in nanowire arrays. *J. Appl. Phys.* **2006,** *100*.
26. Moskowitz, B., Magnetic Force Microscopy Techniques and Applications. International Conference on Rock Magnetism and its Earth Science Applications. **2008**.
27. Magnetic Force Microscopy: Quantitative Results Treatment. *http://www.ntmdt.com/spm-basics/view/quantitative-treatmnet-mfm.*

28. Characterization and calibration o f MFM tip. Quantitative measurements in Magnetic Force Microscopy. *http://www.ece.nus.edu.sg/stfpage/elewuyh/News/mfm_cali.pdf*.
29. Sievers, S.; Braun, K.F.; Eberbeck, D.; Gustafsson, S.; Olsson, E.; Schumacher, H.W.; Siegner, U., Quantitative measurement of the magnetic moment of individual magnetic nanoparticles by magnetic force microscopy. *Small* **2012,** *8*, 2675-2679.
30. Budker, D.; Romalis, M., Optical magnetometry. *Nature Physics* **2007,** *3*, 227-234.
31. Robinson, H.; Ensberg, E.; Dehmelt, H., Preservation of spin state in free atom-inert surface collisions. *Bull. Am. Phys. Soc* **1958,** *3*.
32. Alexandrov, E. B. et all, Light-induced desorption of alkali-metal atoms from paraffin coating. *Phys. Rev.* **2002,** *66*.
33. Groeger, S; Pazgalev, A. S.; Weis, A., Comparison of discharge lamp and laser pumped cesium magnetometers. . *Appl. Phys. B* **2005,** *80*, 645-654.
34. The Spin Exchange Relaxation Free (SERF) Magnetometer. *Romalis Group Home.* **2003.** *http://physics.princeton.edu/romalis/magnetometer/*
35. Schirhagl, R; Kevin, C.; Loretz, M.; Degen, Ch.L., Nitrogen-Vacancy Centers in Diamond: Nanoscale Sensors for Physics and Biology. *Annu. Rev. Phys. Chem.* **2014,** *65*, 83-105.
36. Lim, K; Roop, Ch.; Shapiro, B.; Taylor, J.M.; Wasks, E., Scanning localized magnetic fields in a microfluidic device using single spin in a nano-diamond. *Quant-ph.* **2014**.
37. Kwasi, B., Optical and Spin properties of Nitrogen Vacancy Centers in Bulk and Nanocrystalline Diamond *Thesis.* **2013**.
38. Adur, R., Using single nitrogen-vacancy centers in diamond nanocrystals for sensitive sensing of weak magnetic fields with nanoscale resolution. **2013**.
39. Häberle, T; Schmidt-Lord, D.; Karrai,K.; Reinhard,F.; Wrachtrup, J., High-dynamic-range imaging of nanoscale magnetic fields using optimal control of a single qubit. *Phys. Rev. Lett.* **2013,** *111*.
40. Degen, C. L., Scanning magnetic field microscope with a diamond single-spin sensor. *Appl. Phys. Lett.* **2008,** *92*.
41. Boukallel, M.; Piat, E.; Abadie, J., Passive diamagnetic levitation: theoretical found and applications to the deisign of micro-nano force sensor. *International Conference on Intelligent Robot and Systems* **2003,** *IROS´2003*, 1062-1067.
42. Abadie, J.; Piat, E.; Oster, S.; Boukallel, M., Modeling and experimentation of a passive low frequency nanoforce sensor based on diamagnetic levitation. *Sensors and Actuators* **2012,** *173*, 227-237.
43. Green, R., Hall Effect Measurements in Materials Characterization. *Keithley Instruments, Inc.* **2011**.
44. Pengra, D. B.; Stoltenberg, J.; Van Dyck, R.; Vilches, O., The Hall Effect. **2007**. *http://courses.washington.edu/phys431/hall_effect/hall_effect.pdf*
45. *http://www.analog.com/static/imported-files/data_sheets/AMP04.pdf.* **2000**.
46. Darling, R. B., *http://users.wfu.edu/ucerkb/Nan242/L15-Photolithography.pdf.*